The size distribution of galaxies in the Sloan Digital Sky Survey

Shiyin Shen[1,2], H.J. Mo[1], Simon D.M. White[1], Michael R. Blanton[3],

Guinevere Kauffmann[1], Wolfgang Voges[2], J. Brinkmann[4], Istvan Csabai[4] ⋆

[1] *Max-Planck-Institut für Astrophysik, Karl Schwarzschilddirectory Str. 1, Postfach 1317, 85741 Garching, Germany*

[2] *Max-Planck-Institut für extraterrestrische Physik, Postfach 1312, 85741 Garching, Germany*

[3] *Center for Cosmology and Particle Physics, Department of Physics, New York University, 4 Washington Place,*

New York, NY 10003, USA

[4] *Apache Point Observatory, P.O. Box 59, Sunspot, NM 88349, USA*

2 February 2008

ABSTRACT

We use a complete sample of about 140,000 galaxies from the Sloan Digital Sky Survey (SDSS) to study the size distribution of galaxies and its dependence on their luminosity, stellar mass, and morphological type. The large SDSS database provides statistics of unprecedented accuracy. For each type of galaxy, the size distribution at given luminosity (or stellar mass) is well described by a log-normal function, characterized by its median $\bar{R}$ and dispersion $\sigma_{\ln R}$. For late-type galaxies, there is a characteristic luminosity at $M_{r,0} \sim -20.5$ (assuming $h = 0.7$) corresponding to a stellar mass $M_0 \sim 10^{10.6}$ M$_\odot$. Galaxies more massive than M_0 have $\bar{R} \propto M^{0.4}$ and $\sigma_{\ln R} \sim 0.3$, while less massive galaxies have $\bar{R} \propto M^{0.15}$ and $\sigma_{\ln R} \sim 0.5$. For early-type galaxies, the $\bar{R}$ - M relation is significantly steeper, $\bar{R} \propto M^{0.55}$, but the $\sigma_{\ln R}$ - M relation is similar to that of bright late-type galaxies. Faint red galaxies have sizes quite independent of their luminosities. We use simple theoretical models to interpret these results. The observed $\bar{R}$ - M relation for late-type galaxies can be explained if the fraction of baryons that form stars is as predicted by the standard feedback model. Fitting the observed $\sigma_{\ln R}$ -

⋆ E-mail: shen@mpa-garching.mpg.de

M relation requires in addition that the bulge/disk mass ratio be larger in haloes of lower angular momentum and that the bulge material transfer part of its angular momentum to the disk. This can be achieved if bulge formation occurs so as to maintain a marginally stable disk. For early-type galaxies the observed $\sigma_{\ln R}$ - M relation is inconsistent with formation through single major mergers of present-day disks. It is consistent with formation through repeated mergers, if the progenitors have properties similar to those of faint ellipticals or Lyman break galaxies and merge from relatively strongly bound orbits.

1   INTRODUCTION

Luminosity, size, circular velocity (or velocity dispersion), and morphological type are the most basic properties of a galaxy. Observed galaxies cover large ranges in these properties, with luminosities between $\sim 10^8\,\mathrm{L}_\odot$ and $\sim 10^{12}\,\mathrm{L}_\odot$, effective radii between $\sim 0.1\,\mathrm{kpc}$ and $\sim 10\,\mathrm{kpc}$, circular velocity (or velocity dispersion) between $\sim 30\,\mathrm{km\,s^{-1}}$ and $\sim 300\,\mathrm{km\,s^{-1}}$, morphologies changing from pure disk systems to pure ellipsoidal systems. Clearly, the study of the distribution of galaxies with respect to these properties and the correlation among them are crucial to our understanding of the formation and evolution of the galaxy population.

There has been much recent progress in this area. For example, the luminosity function of galaxies has been measured from various redshift surveys of galaxies and is found to be well described by the Schechter function (Schmidt 1968; Loveday et al. 1992; Lin et al. 1996; Folkes et al. 1999; Madgwick et al. 2002); the morphological type of galaxies is found to be correlated with their local environment (as reflected in the the morphology-density relation, Dressler 1980; Dressler et al. 1997) and other properties (e.g. Roberts & Haynes 1994); and galaxy sizes are correlated with luminosity and morphological type (Kormendy 1977), and have a distribution which may be described by a log-normal function (Choloniewski 1985; Syer, Mao & Mo 1999; de Jong & Lacey 2000).

Clearly, in order to examine these properties in detail, one needs large samples of galaxies with redshift measurements and accurate photometry. The Sloan Digital Sky Survey (SDSS, York et al. 2000), with its high-quality spectra and good photometry in five bands for $\sim 10^6$ galaxies, is providing an unprecedented database for such studies. The survey is ongoing, but the existing data are providing many interesting results about the distribution

of galaxies with respect to their intrinsic properties. The luminosity function has been derived by Blanton et al. (2001, 2002c) and the dependence of luminosity function on galaxy type has been analyzed by Nakamura et al. (2003). Shimasaku et al. (2001), Strateva et al. (2002) and Nakamura et al. (2003) have examined the correlation between galaxy morphological type and other photometric properties, such as color and image concentration. The fundamental-plane and some other scaling relations of early-type galaxies have been investigated by Bernardi et al. (2003a, 2003b, 2003c). Based on a similar data set, Sheth et al. (2003) have studied the distribution of galaxies with respect to central velocity dispersion of galaxies. By modelling galaxy spectra in detail, Kauffmann et al. (2002a) have measured stellar masses for a sample of more than 10^5 galaxies, and have analyzed the correlation between stellar mass, stellar age and structural properties determined from the photometry (Kauffmann et al. 2002b). Blanton et al. (2002b) have examined how various photometric properties of galaxies correlate with each other and with environment density.

In this paper, we study in detail the size distribution of galaxies and its dependence on galaxy luminosity, stellar mass and morphological type. Our purpose is twofold: (1) to quantify these properties so that they can be used to constrain theoretical models; (2) to use simple models based on current theory of galaxy formation to interpret the observations. Some parts of our analysis overlap that of Blanton et al. (2002b), Kauffmann et al. (2002b) and Bernardi et al. (2003b), but in addition we address other issues. We pay considerable attention to effects caused by the sample surface brightness limit and by seeing, we provide detailed fits to the data to quantify the dependence of the size distribution on other galaxy properties, and we discuss how these results can be modelled within the current theory of galaxy formation.

Our paper is organized as follows. In Section 2, we describe the data to be used. In Section 3, we derive the size distribution of galaxies as a function of luminosity, stellar mass, and type. In Section 4, we build simple theoretical models to understand the observational results we obtain. Finally, in Section 4, we summarize our main results and discuss them further.

2   THE DATA

In this section, we describe briefly the SDSS data used in this paper. These data are of two types: the basic SDSS photometric and spectroscopic data, and some quantities derived by our SDSS collaborators from the basic SDSS database.

2.1   The basic SDSS data

The SDSS observes galaxies in five photometric bands (u, g, r, i, z) centred at (3540, 4770, 6230, 7630, 9130Å) down to 22.0, 22.2, 22.2, 21.3, 20.5 mag, respectively. The imaging camera is described by Gunn et al. (1998); the filter system is roughly as described in Fukugita et al. (1996); the photometric calibration of the SDSS imaging data is described in Hogg et al. (2001) and Smith et al. (2002); and the accuracy of astrometric calibration is described in Pier et al. (2003). The basic SDSS photometric data base is then obtained from an automatic software pipeline called **Photo** (see Lupton et al. 2001, 2002), whereas the basic spectroscopic parameters of each galaxy, such as redshift, spectral type, etc, are obtained by the spectroscopic pipelines **idlspec2d** (written by D. Schlegel & S. Burles) and **spectro1d** (written by M. SubbaRao, M. Bernardi and J. Frieman). Many of the survey properties are described in detail in the Early Data Release paper (Stoughton et al. 2002, hereafter EDR).

Photo uses a modified form of the Petrosian (1976) system for galaxy photometry, which is designed to measure a constant fraction of the total light independent of the surface-brightness limit. The Petrosian radius r_P is defined to be the radius where the local surface-brightness averaged in an annulus equals 20 percent of the mean surface-brightness interior to this annulus, i.e.

$$\frac{\int_{0.8r_P}^{1.25r_P} dr 2\pi r I(r)/[\pi(1.25^2 - 0.8^2)r^2]}{\int_0^{r_P} dr 2\pi r I(r)/[\pi r^2]} = 0.2, \tag{1}$$

where $I(r)$ is the azimuthally averaged surface-brightness profile. The Petrosian flux F_p is then defined as the total flux within a radius of $2r_P$,

$$F_p = \int_0^{2r_P} 2\pi r dr I(r). \tag{2}$$

With this definition, the Petrosian flux (magnitude) is about 98 percent of the total flux for an exponential profile and about 80 percent for a de Vaucouleurs profile. The other two Petrosian radii listed in the **Photo** output, R_{50} and R_{90}, are the radii enclosing 50 percent and 90 percent of the Petrosian flux, respectively. The concentration index c, defined as

$c \equiv R_{90}/R_{50}$, is found to be correlated with galaxy morphological type (Shimasaku et al. 2001; Strateva et al. 2002; Nakamura et al. 2003). An elliptical galaxy with a de Vaucouleurs profile has $c \sim 3.3$ while an exponential disk has $c \sim 2.3$. Note that these **Photo** quantities are not corrected for the effects of the point spread function (hereafter PSF) and, therefore, for small galaxies under bad seeing conditions, the Petrosian flux is close to the fraction measured within a typical PSF, about 95% for the SDSS (Blanton et al. 2001). In such cases, the sizes of compact galaxies are over-estimated, while their concentration indices are under-estimated by the uncorrected **Photo** quantities (Blanton et al. 2002b).

The SDSS spectroscopic survey aims to obtain a galaxy sample complete to $r \sim 17.77$ in the r-band (Petrosian) magnitude and to an average r-band surface-brightness (within R_{50}) $\mu_{50} \sim 24.5$ magarcsec^{-2}. This sample is denoted the Main Galaxy Sample, to distinguish it from another color-selected galaxy sample, the Luminous Red Galaxies (LRGs), which extends to $r \sim 19.5$ (Eisenstein et al. 2001). These target selections are carried out by the software pipeline **target**; details about the target selection criteria for the Main Galaxy Sample are described in Strauss et al. (2002). The tiling algorithm of the fibers to these spectroscopic targets is described in Blanton et al. (2003).

The spectroscopic pipelines, **idlspec2d** and **spectro1d**, are designed to produce fully calibrated one-dimensional spectra, to measure a variety of spectral features, to classify objects by their spectral types, and to determine redshifts. The SDSS spectroscopic pipelines have an overall performances such that the correct classifications and redshifts are found for 99.7% of galaxies in the main sample (Strauss et al. 2002). The errors in the measured redshift are typically less than $\sim 10^{-4}$.

2.2 Derived quantities for SDSS galaxies

In the SDSS **Photo** output, the observed surface-brightness profiles of galaxies are given in **profMean** where angle averaged surface-brightness in a series of annuli are listed (see EDR). Blanton et al. (2002b) fitted the angle averaged profiles with the Sérsic (1968) model,

$$I(r) = I_0 \exp\left[-(r/r_0)^{1/n}\right], \tag{3}$$

convolved with the PSF, to obtain the central surface-brightness I_0, the scale radius r_0, and the profile index n for each galaxy. As found by many authors (e.g. Trujillo, Graham & Caon 2001 and references therein), the profile index n is correlated with the morphological type, with late-type spiral galaxies (whose surface-brightness profiles can be approximated

by an exponential function) having $n \sim 1$, and early-type elliptical galaxies (whose surface-brightness profiles can be approximated by the $r^{1/4}$ function) having $n \sim 4$. From the fitting results, one can obtain the total Sérsic magnitude (flux), the Sérsic half-light radius, $R_{50,S}$, and other photometric quantities. In our following analysis, we will use these quantities and compare the results so obtained with those based on the original **Photo** quantities. For clarity, we denote all the Sérsic quantities by a subscript 'S'. We present results for both Petrosian and Sérsic quantities, because while the Sérsic quantities are corrected for seeing effect, the Petrosian quantities are the standard photometric quantities adopted by the SDSS community.

Recently, Kauffmann et al. (2002a) developed a method to estimate the stellar mass of a galaxy based on its spectral features, and obtained the stellar masses for a sample of 122,808 SDSS galaxies. The 95% confidence range for the mass estimate of a typical galaxy is $\pm 40\%$. Below we use these results to quantify size distributions as a function of stellar mass as well as a function of luminosity.

2.3   Our sample

The main sample we use in this paper is a sub-sample of the spectroscopic targets observed before April 2002, which is known as the Large-Scale Structure (LSS) **sample10** within the SDSS collaboration (Blanton et al. 2002c). We select from it 168,958 Main Galaxy Targets (with SDSS flag TARGET_GALAXY or TARGET_GALAXY_BIG) with high-confidence redshifts (**zWarning = 0**).

Figure 1 shows histograms of the basic quantities of our selected sample. The top-right panel shows the galaxy distribution in r-band apparent magnitude r after correction for foreground Galactic extinction using the reddening map of Schlegel, Finkbeiner and Davis (1998). The abrupt cut at ~ 17.77 mag is caused by the target selection criteria. The top-left panel shows the distribution of the r-band Petrosian half-light radius $R_{50,r}$. The distribution of $\mu_{50,r}$, the r-band average surface-brightness within $R_{50,r}$, is shown in the bottom-left panel. Since the r-band is the reference band of the SDSS for model fitting and target selection, our discussion of sample incompleteness will be based on the photometric properties in this band. The redshifts z of the sample galaxies are obtained from the spectroscopic data, and the distribution of galaxies with respect to z is shown in the bottom-right panel of Figure 1.

All the galaxies in this sample have Sérsic parameters given by Blanton et al. (2002b).
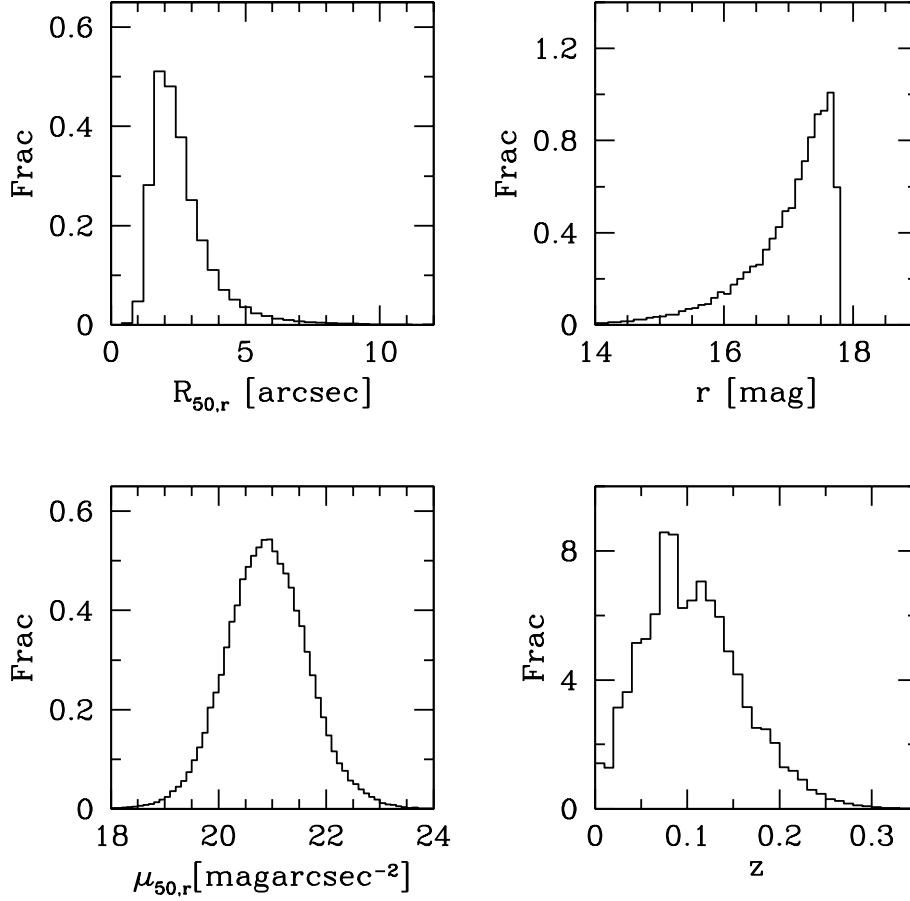
Figure 1. The distribution of galaxies with respect to some basic SDSS photometric quantities and the redshift. All histograms are normalized to 1.

The stellar mass sample by Kauffmann et al. (2002a) contains objects spectroscopically classified as galaxies, with magnitude in the range $14.5 < r < 17.77$, selected from all available spectroscopic observations in the SDSS upcoming Data Release One (DR1). The area covered by this stellar mass sample is almost all contained within our sample, and we obtain a subsample of 118,850 galaxies with stellar masses. This subsample has the same properties as the main sample except the smaller sky coverage.

To study the size distribution of galaxies, we need to define a complete sample for which selection effects can be corrected. As discussed in Strauss et al. (2002), the stable **target** version gives an almost complete sample in the magnitude range $15.0 \leq r \leq 17.77$ and with surface-brightness $\mu_{50} \leq 24.5$ magarcsec^{-2}. However, during the commissioning of SDSS, a number of tentative versions of **target** were used for refining the final **target** algorithms,

and the trial **target**s have small differences in the magnitude and surface-brightness limits (see EDR for detail). Therefore, to define a complete sample we need to consider selection effects in more detail. Because galaxies with $23.0 \, \mathrm{magarcsec}^{-2} < \mu_{50} < 24.5 \, \mathrm{magarcsec}^{-2}$ are targeted only when the local and global sky values are within $0.05 \, \mathrm{magarcsec}^{-2}$ (Strauss et al. 2002), we set a lower surface-brightness limit at $\mu_{\mathrm{lim}} = 23.0 \, \mathrm{magarcsec}^{-2}$. As one can see from the bottom-left panel of Fig. 1, the total number excluded by this selection criterion is very small. Next, to avoid the contamination by bright stars, **target** rejects bright compact objects with $R_{50} < 2''$ and $r < 15.0$ (15.5 in **target** v_2_7). Because of this, we exclude all galaxies brighter than 15.0 (15.5 for objects targeted by **target** v_2_7). As shown in Fig. 1, only a small number of galaxies are excluded by this criterion also. Finally, the magnitude limit (r_{max}) at the faint end varies across the sky in different versions of **target**. We take this into account by treating r_{max} as a function of sky position (θ, ϕ).

A more important effect is that some galaxies are so small (compact) that either their size measurements are seriously affected by the PSFs, or they are misclassified as stars by **target**. As discussed by Strauss et al. (2002), very few true galaxies at the compact end are missed by the target criteria. However, to take care of the seeing effects, we use only galaxies with angular sizes $R_{50} > D_{\mathrm{min}}$, and we choose $D_{\mathrm{min}} = 1.6''$ (i.e. 4 pixels). This choice, based on the fact that the median seeing condition in SDSS is about $1.5''$, is conservative, because the PSF is known quite accurately. In practice, this cut does not affect our results, as only a relatively small fraction of galaxies is excluded (see the top-left panel of Fig.1). Finally we also exclude a small number of galaxies with redshift $z < 0.005$, whose distances may be severely contaminated by their peculiar velocities. In summary, our final complete sample includes all galaxies with $\mu_{50} \leq 23.0 \, \mathrm{magarcsec}^{-2}$, $r_{\mathrm{min}}(\theta, \phi) \leq r \leq r_{\mathrm{max}}(\theta, \phi)$, $R_{50} \geq 1.6''$ and $z \geq 0.005$. This sample contains 138,521 galaxies, of which 99,786 have stellar masses.

2.4 Subsamples of galaxy types

In this paper we also wish to analyze the dependence of the size distribution on galaxy type, so we need to adopt some criteria to classify galaxies.

There are attempts to classify SDSS galaxies into morphological classes through direct inspection of the galaxy images (Shimasaku et al. 2001; Nakamura et al. 2003). While such eye-ball classification should match the original Hubble morphological sequence, it is quite tedious and has so far been carried out only for about 1500 big galaxies in the SDSS. However,

it has been suggested that some photometric and spectroscopic properties may be closely correlated with the morphological type, and so can be used as morphology indicators. For example, Shimasaku et al. (2001) show that the concentration c can be used to separate early-type (E/S0) galaxies from late-type (Sa/b/c, Irr) galaxies. Using about 1500 galaxies with eye-ball classifications, Nakamura et al. (2003) confirmed that $c = 2.86$ separates galaxies at S0/a with a completeness of about 0.82 for both late and early types. For the Sérsic profile (Blanton et al. 2002b), the profile index n is uniquely related to the concentration parameter, and so the value of n may also serve as a morphological indicator. Other profile indicators of galaxy type include the exponential and de Vaucouleurs profile likelihoods, P_{exp} and P_{dev}, given in the **Photo** output. Based on the broad band colors, Strateva et al. (2002) suggested that the color criterion $u^* - r^* > 2.22$ can separate early types (E/S0/Sa) from late types (Sb/Sc/Irr). Blanton et al. (2002b) found that the color criteria $^{0.1}(g-r) \sim 0.7$ [where $^{0.1}(g-r)$ is the $g-r$ color K-corrected to the redshift of 0.1] separates galaxies into two groups with distinct properties. There are also attempts to classify SDSS galaxies according to their spectral types, such as that based on the Principal Component Analysis (Yip et al. 2003) and that on the 4000Å spectral break index (Kauffmann et al. 2002b). It must be pointed out, however, that all these simple type classifications have uncertainties and are only valid in the statistical sense. For example, the profile and color indices can both be affected by dust extinction, while the classifications based on spectra can be affected aperture biases due to the finite ($3''$ in diameter) of the fibers. Because of these uncertainties, we only divide galaxies into a small number of subsamples according to types. More specifically, we use $c = 2.86$ and $n = 2.5$ as two basic indicators to separate galaxies into early and late types. With such a separation, most Sa galaxies are included in the late-type category. We also use the color criterion, $^{0.1}(g-r) = 0.7$ for comparison. The n separation is set at 2.5, the average between exponential profile ($n = 1$) and de Vaucouleurs profile ($n = 4$), which also gives an early/late ratio similar to that given by the separator $c = 2.86$. We adopt the $^{0.1}(g-r)$ color rather than the $u^* - r^*$ color, because the g-band photometry is currently better than the u-band photometry in the SDSS and because the K-correction for the u-band is very uncertain.

3   THE SIZE DISTRIBUTION OF GALAXIES

In this section, we derive the size distribution as a function of luminosity and stellar mass for galaxies of different types. Specifically, we first bin galaxies of a given type into small bins of absolute magnitude (or mass). We then use a V_{max} method to make corrections for the incompleteness due to selection effects, and derive the conditional size distribution function $f_i(R|M_i)$ for a given bin. Finally, we investigate the size distribution as a function of luminosity (or stellar mass).

3.1   The V_{max} correction of the selection effects

As described in the last section, our sample is selected to be complete only to some magnitude, size and surface-brightness limits. In order to obtain the size distribution for the galaxy population as a whole, we must make corrections for these selection effects. In this paper we use the V_{max} method to do this.

The basic idea of the V_{max} method is to give each galaxy a weight which is proportional to the inverse of the maximum volume (V_{max}) within which galaxies identical to the one under consideration can be observed. For a given galaxy with magnitude r, Petrosian half-light radius R_{50}, surface-brightness μ_{50}, and redshift z, the selection criteria described in the last section define the value of V_{max} in the following way. First, the magnitude range $r_{min} \leq r \leq r_{max}$ corresponds to a maximum redshift $z_{max,m}$ and a minimum redshift $z_{min,m}$:

$$d_L(z_{max,m}) = d_L(z)10^{-0.2(r-r_{max})}; \; d_L(z_{min,m}) = d_L(z)10^{-0.2(r-r_{min})}, \tag{4}$$

where $d_L(z)$ is the luminosity distance at redshift z. Note that we have neglected the effects of K-correction and luminosity evolution in calculating $d_L(z_{max,m})$ and $d_L(z_{min,m})$. In general, the K-correction make a given galaxy fainter in the observed r-band if it is put at higher redshift. The luminosity evolution has an opposite effect; it makes galaxies brighter at higher redshift. We found that including these two opposing effects (each is about one magnitude per unit redshift, see Blanton et al. 2002a; 2002c) has a negligible impact on our results.

The surface-brightness limit constrains the V_{max} of a galaxy mainly through the dimming effect. The maximum redshift at which a galaxy of surface-brightness μ_{50} at z can still be observed with the limit surface-brightness $\mu_{lim} = 23.0$ is given by

$$z_{max,\mu} = (1+z)10^{\frac{(23.0-\mu_{50})}{10}} - 1. \tag{5}$$

Here, again, K-correction and luminosity evolution are neglected. We have also neglected

possible color gradients in individual galaxies. The minimum size limit D_{min} also defines a maximum redshift $z_{max,R}$ given by

$$\frac{d_A(z_{max,R})}{d_A(z)} = \frac{R_{50}}{1.6''},\tag{6}$$

where d_A is the angular-diameter distance. The real maximum and minimum redshifts, z_{max} and z_{min}, for a given galaxy are therefore given by

$$z_{min} = \max(z_{min,m}, 0.005)\,;\ z_{max} = \min(z_{max,m}, z_{max,\mu}, z_{max,R}),\tag{7}$$

and the corresponding V_{max} is

$$V_{max} = \frac{1}{4\pi}\int d\Omega f(\theta,\phi)\int_{z_{min}(\theta,\phi)}^{z_{max}(\theta,\phi)}\frac{d_A^2(z)}{H(z)(1+z)}c\,dz\,,\tag{8}$$

where $H(z)$ is the Hubble constant at redshift z, c is the speed of light, $f(\theta,\phi)$ is the sampling fraction as a function of position on the sky, and Ω is the solid angle.

The apparent-magnitude limit only influences the number of galaxies at a given absolute-magnitude, and so it does not matter when we analyze the size distribution for galaxies with a given absolute magnitude. We can define a 'conditional' maximum volume,

$$V_{max}^* = \frac{V_{max}}{(4\pi)^{-1}\int d\Omega f(\theta,\phi)\int_{z_{min}(\theta,\phi)}^{z_{max,m}(\theta,\phi)}d_A^2(z)H^{-1}(z)(1+z)^{-1}c\,dz}\tag{9}$$

which takes values from 0 to 1, and gives the probability a galaxy with size R_{50} can be observed at the given absolute magnitude. Given N galaxies in an absolute-magnitude (or mass) bin $M \pm \Delta M$, the intrinsic conditional size distribution $f(R|M)$ can be estimated from

$$f(R|M) \propto \sum_{i=1}^{N}\frac{1}{V_{max,i}^*}\quad\text{if } R - dR < R_i < R + dR,\tag{10}$$

where R_i and $V_{max,i}^*$ are the radius and the value of V_{max}^* for the ith galaxy.

3.2 Size distribution: dependence on luminosity

In this subsection, we study the size distribution as a function of luminosity for galaxies of different type. The absolute magnitude M is calculated from the observed apparent magnitude m using

$$M = m - DM(z) + 5 - K(z),\tag{11}$$

where z is the redshift of the galaxy, $DM(z)$ is the distance modulus and $K(z)$ is the K-correction. The distances are calculated from redshifts using a cosmology with mass density
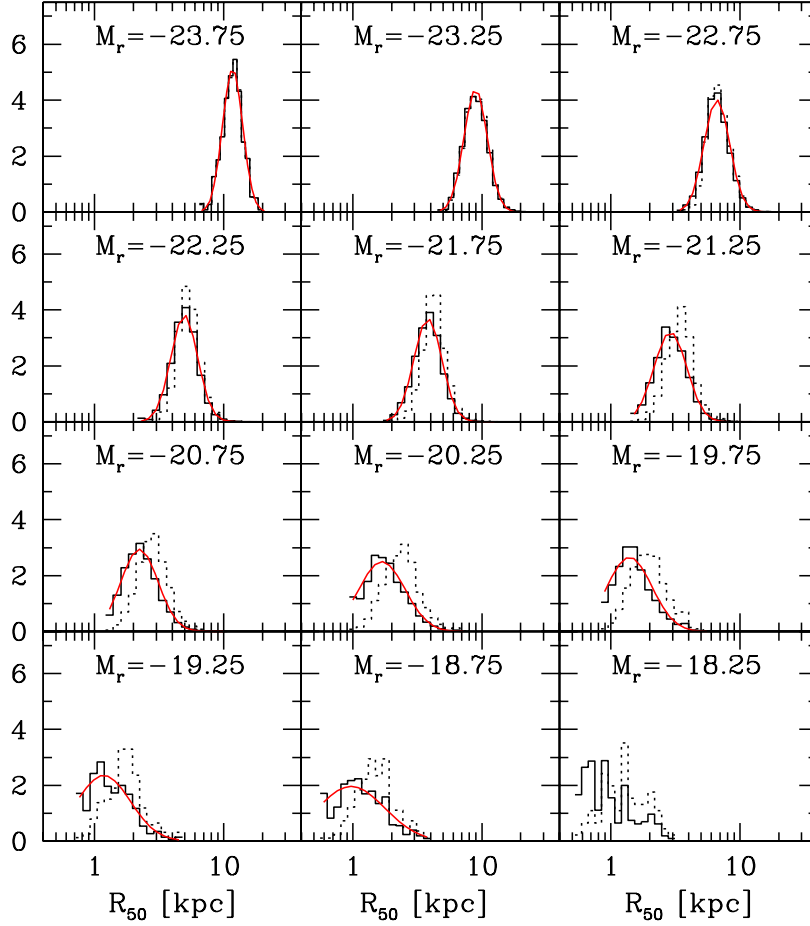
Figure 2. Histograms of Petrosian half-light radius R_{50} (in the r-band) for early-type ($c > 2.86$) galaxies in different Petrosian r-band absolute-magnitude bins. The dotted histograms show the raw distribution, while the solid histograms show the results after V_{max} correction for selection effects. The solid curves are obtained by fitting the sizes to a log-normal distribution through the maximum-likelihood method.

$\Omega_0 = 0.3$, cosmological constant $\Omega_\Lambda = 0.7$, and Hubble's constant $h = 0.7$. The K-correction is calculated based on the study of Blanton et al. (2002a).

In Figures 2 and 3 we show the histograms of Petrosian half-light radius R_{50} for galaxies of different absolute magnitudes and types. We use $c = 2.86$ to separate galaxies, in which case 32 percent of them are included in the early types. Galaxies of a given type are further divided into absolute-magnitude bins with a width of 0.5 mag. The dotted histograms show the observed size distributions, obtained by directly counting the numbers of galaxies in given size bins. The intrinsic distributions, obtained by using the V_{max}^* correction [see equation (10)], are shown as the solid histograms. All the histograms are normalized to the unit area in the space of Log (R_{50}).
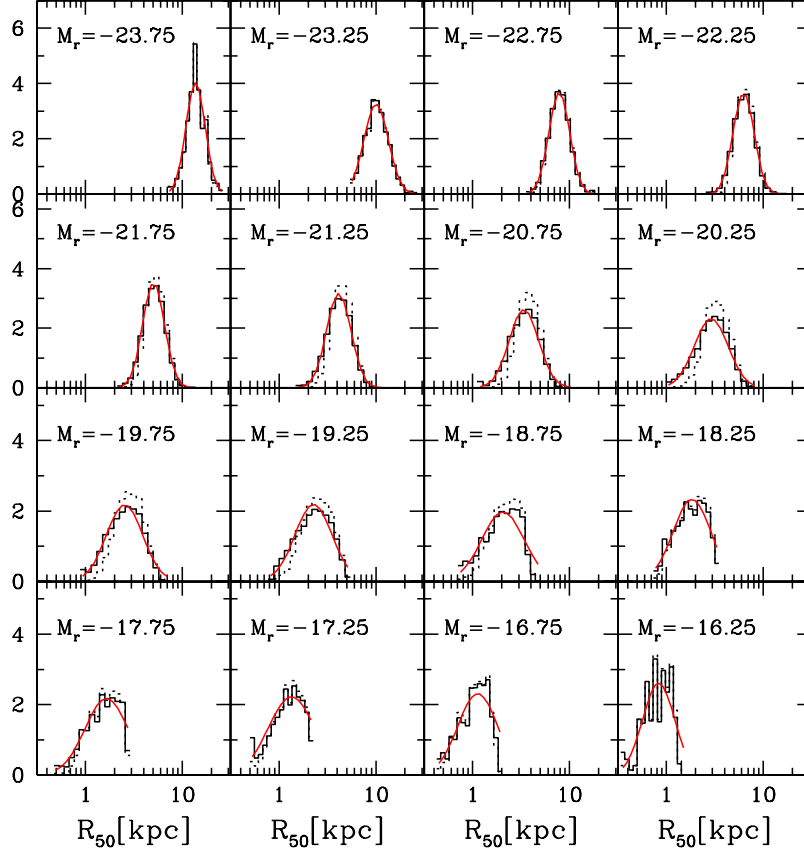
Figure 3. The same as Fig.2, but for late-type ($c < 2.86$) galaxies.

As one can see, for both late- and early-type galaxies, the intrinsic size distributions can be approximated reasonably well by a log-normal function. As we will see later, this type of distribution in sizes is also motivated by theoretical considerations. We therefore make the assumption that $f(R|M)$ has a log-normal form,

$$f(R, \bar{R}(M), \sigma_{\ln R}(M)) = \frac{1}{\sqrt{2\pi}\sigma_{\ln R}(M)} \exp\left[-\frac{\ln^2(R/\bar{R}(M))}{2\sigma_{\ln R}^2(M)}\right] \frac{dR}{R}, \quad (12)$$

which is characterized by the median $\bar{R}(M)$ and the dispersion $\sigma_{\ln R}(M)$. We use a maximum likelihood method to estimate $\bar{R}$ and $\sigma_{\ln R}$ at each magnitude bin. The procedure goes as follows. For a sample of N galaxies (in a certain absolute-magnitude bin) with sizes $\{R_i\}_{i=1,N}$ and conditional maximum volumes $\{V_{\max,i}^*\}_{i=1,N}$, the likelihood for the size distribution is

$$\mathcal{L}(\bar{R}, \sigma_{\ln R}) = \prod_{i=1}^{N} \frac{1}{V_{\max,i}^*} \frac{f(R_i, \bar{R}, \sigma_{\ln R})dR}{\int_{R_{\min}}^{R_{\max}} f(R, \bar{R}, \sigma_{\ln R})dR}, \quad (13)$$
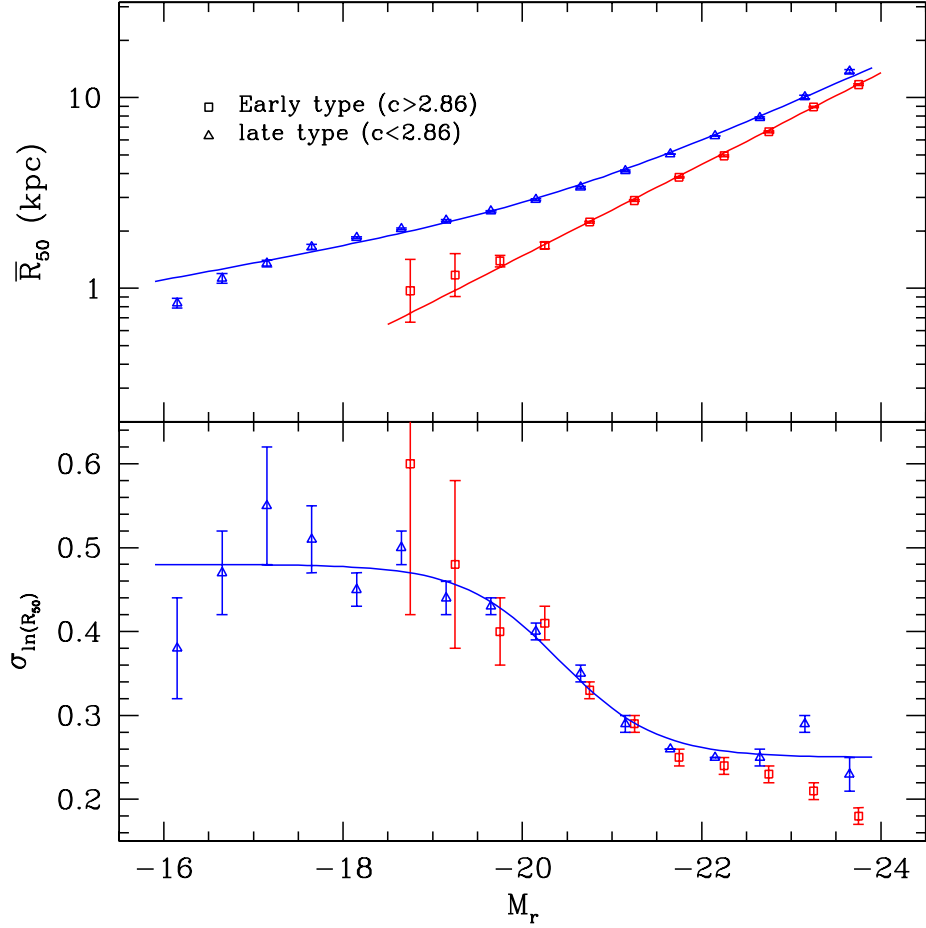
Figure 4. The median and dispersion of the distribution of Petrosian half-light radius R_{50} (in the r-band), as functions of r-band Petrosian absolute magnitude, obtained by fitting a log-normal function. Results for late-type ($c < 2.86$) and early-type ($c > 2.86$) galaxies are shown as triangles and squares, respectively. The error bars represent the scatter among 20 bootstrap samples. The solid curves are the fit of the $\bar{R}$ - M and $\sigma_{\ln R}$ - M relations by equations (14), (15) and (16).

where $R_{\min}$ and $R_{\max}$ are the minimum and maximum radii that can be observed for the luminosity bin in consideration, $f(R, \bar{R}, \sigma_{\ln R})$ is the log-normal function with median $\bar{R}$ and dispersion $\sigma_{\ln R}$ given in equation (12). By maximizing this likelihood function, we obtain the best estimates of $\bar{R}$ and $\sigma_{\ln R}$ for each magnitude bin. The solid curves in Figures 2 and 3 show the results of the log-normal functions so obtained. As one can see, they provide very good fits to the solid histograms.

Figure 4 shows $\bar{R}$ (upper panel) and $\sigma_{\ln R}$ (lower panel) against the absolute magnitude. Triangles and squares denote the results for late- and early-type galaxies, respectively. The error bars are obtained from the scatter among 20 bootstrap samples. The small error bars show the statistics one can get from the current sample. The number of faint early-type

galaxies is still too small to give any meaningful results (see the panel of $M_r = 18.25$ in Fig. 1). This small number may not mean that the number of faint elliptical galaxies is truly small; it may just reflect our definition of early- and late-type galaxies. Indeed, faint elliptical galaxies seem to have surface-brightness profiles better described by an exponential than a $R^{1/4}$ law (Andredakis, Peletier & Balcells 1995; Kormendy & Bender 1996), and so they will be classified as 'late-type' galaxies according to the c criterion because of their small concentration.

As shown in Fig. 4, the dependence of $\bar{R}$ on the absolute magnitude is quite different for early- and late-type galaxies. In general, the increase of $\bar{R}$ with luminosity is faster for early-type galaxies. The $\bar{R}$ - M relation can roughly be described by a single power law for bright early-type galaxies, while for late-type galaxies, the relation is significantly curved, with brighter galaxies showing a faster increase of $\bar{R}$ with M. In the luminosity range where $\bar{R}$ and $\sigma_{\ln R}$ can be determined reliably, the dispersion has a similar trend with M for both early- and late-type galaxies. An interesting feature in $\sigma_{\ln R}$ is that it is significantly smaller for galaxies brighter than -20.5 mag (in the r-band). As we will discuss in Section 4, these observational results have important implications for the theory of galaxy formation.

To quantify the observed $\bar{R}$ - M and $\sigma_{\ln R}$ - M relations, we fit them with simple analytic formulae. For early-type galaxies, we fit $\bar{R}$ - M by,

$$\text{Log}\,(\bar{R}/\,\text{kpc}) = -0.4aM + b\,, \tag{14}$$

where a and b are two fitting constants. For late-type galaxies, we fit the size-luminosity relation and its dispersion by

$$\text{Log}\,(\bar{R}/\,\text{kpc}) = -0.4\alpha M + (\beta - \alpha)\,\text{Log}\,[1 + 10^{-0.4(M-M_0)}] + \gamma \tag{15}$$

and

$$\sigma_{\ln R} = \sigma_2 + \frac{(\sigma_1 - \sigma_2)}{1 + 10^{-0.8(M-M_0)}}\,, \tag{16}$$

where α, β, γ, σ_1, σ_2 and M_0 are fitting parameters. Note that the value of M_0 used in equation (15) is determined by fitting the observed $\sigma_{\ln R}$ - M relation [equation (16)], because the fit of the $\bar{R}$ - M relation is not very sensitive to the value of M_0. Thus, the relation between $\bar{R}$ and the luminosity L is $R \propto L^a$ for early-type galaxies. For late-type galaxies, $R \propto L^\alpha, \sigma_{\ln R} = \sigma_1$ at the faint end ($L \ll L_0$, where L_0 is the luminosity corresponding to M_0), and $R \propto L^\beta, \sigma_{\ln R} = \sigma_2$ at the bright end ($L \gg L_0$). We use the least-square method
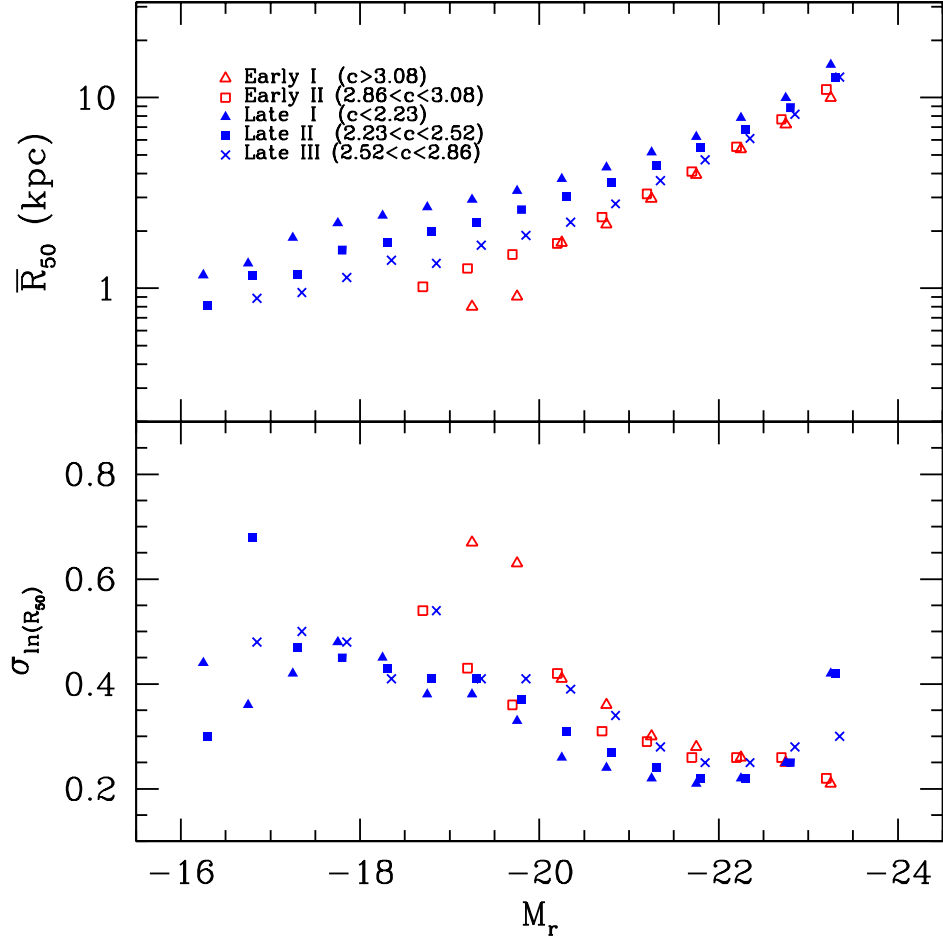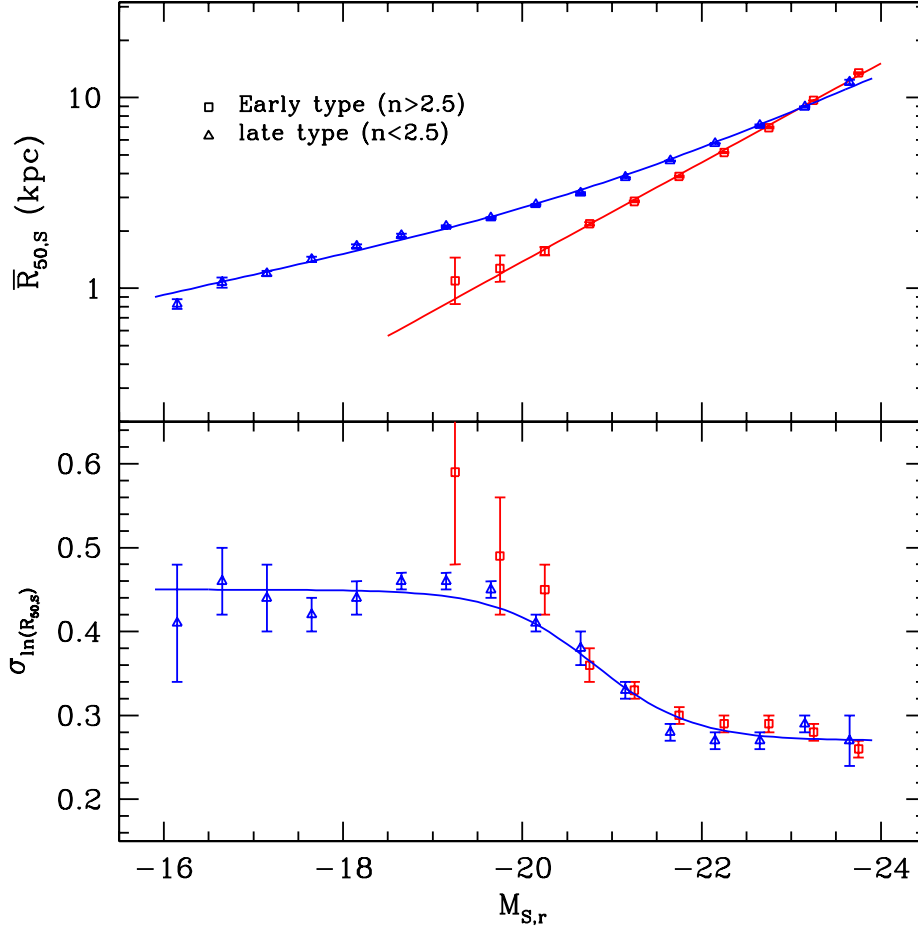
Figure 5. The median and dispersion of the R_{50} (in the r-band) distribution, as a function of r-band Petrosian absolute magnitude, for galaxies in fine bins of c.

to estimate the fitting parameters and the results are given in Table 1. These fit results are also plotted as solid lines in Fig. 4.

We have also analyzed the size distribution as a function of luminosity in finer ranges of c. Specifically, we further divide late-type galaxies ($c < 2.86$) into three sub-samples containing equal numbers of galaxies, and early-type galaxies ($c > 2.86$) into two equal sub-samples. The ranges of c and the results for $\bar{R}$ and $\sigma_{\ln R}$ for these sub-samples are shown in Figure 5. As we can see, the $\bar{R}$ - M relation depends systematically on c: galaxies with higher c show a steeper relation. However, the difference between the two early-type samples is quite small, except for the two faintest bins where the statistic is quite poor.

As discussed in Section 2.2, the Sérsic half-light radii $R_{50,S}$ given by Blanton et al. (2002b) have the merit of being corrected for PSF and, unlike the Petrosian magnitude, the Sérsic

Figure 6. The median and dispersion of the distribution of the Sérsic half-light radius $R_{50,S}$ (in the r-band) as functions of r-band absolute Sérsic magnitude. Here a galaxy is separated into early- or late-type according to whether its Sérsic index n is larger or smaller than 2.5. The error bars represent the scatter among 20 bootstrap samples. The solid curves are the fit of the $\bar{R}$ - M and $\sigma_{\ln R}$ - M relations by equations (14), (15) and (16).

magnitude has also the merit of including the total flux of a galaxy. We therefore also made analyses based on the Sérsic quantities. Here we use $n = 2.5$ to separate late- and early-type galaxies. In this separation, about 36 percent of the galaxies are classified as early types. Figure 6 shows the results of $\bar{R}$ and $\sigma_{\ln R}$ for the Sérsic quantity $R_{50,S}$. We have also fitted the size-luminosity relations to the functional form given by equations (14), (15) and (16), and the fitting parameters are listed in Table 1. Comparing these results with those shown in Fig. 4, we see that early type galaxies here have systemtical bigger half-light radii for given luminosity. This is caused by differences between the Petrosian and Sérsic quantities. For a galaxy with pure de Vaucouleurs profile, the Petrosian magntitude includes about 80 percent of the total flux, while the Petrosian half-light radius is only about 70 percent of the real half-
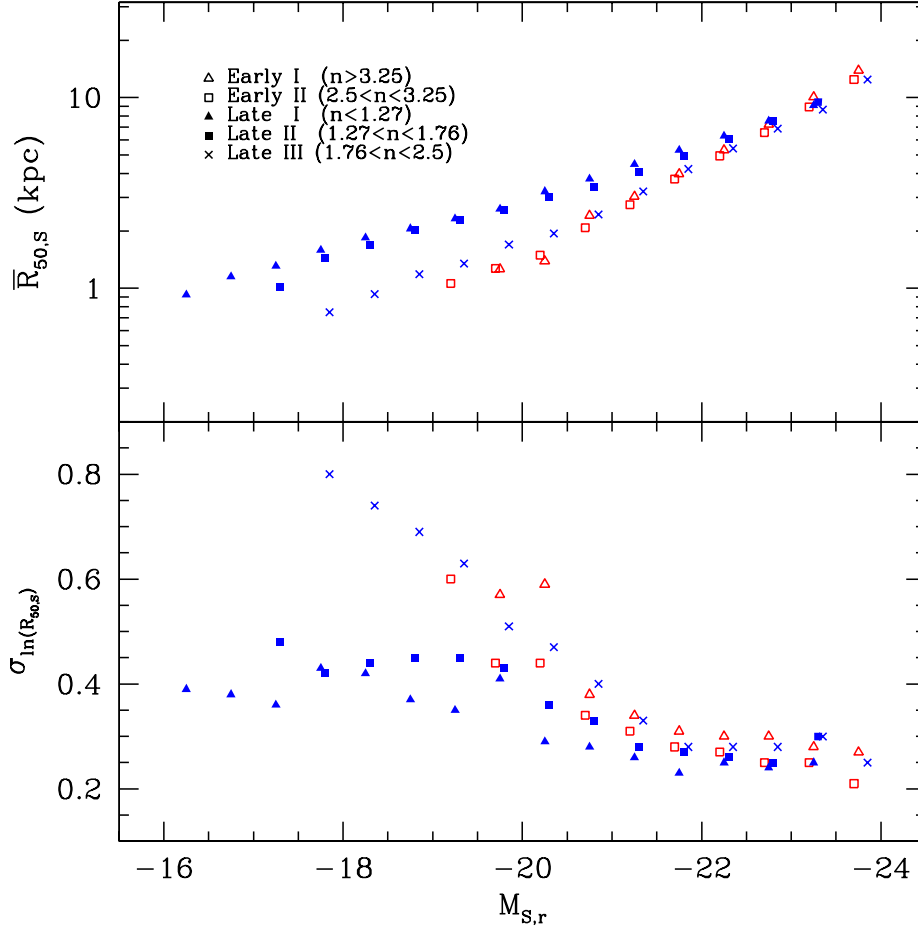
Figure 7. The median and dispersion of the distributions of Sérsic half-light radius, $R_{50,S}$, as functions of r-band absolute Sérsic magnitude, for galaxies in fine bins of the Sérsic index n.

light radius. Note that our derived slopes for the $R - L$ relation in both cases are consitent with the result $R \propto L^{0.63}$ obtained by Bernardi et al. (2003b) where yet another photometric system is used. For late type galaxies with exponential light profiles, no significant difference is found between these these two systems, because the Petrosian magnitude includes almost all the total flux and the half light radius is approximately the same as the true half light radius. Although our results show a significant curved $R - L$ relation for late type galaxies, a simple power law is usually used as an assumption in previous studies due to the small samples. But the results are generally consistent, for example, the relation gotten by de Jong & Lacey(2000) is $R \propto L^{0.25}$ in I band.

Expanding on this, we have analyzed the size distribution as a function of luminosity in finer bins of n. We divide the late-type sample ($n < 2.5$) into three equal sub-samples,
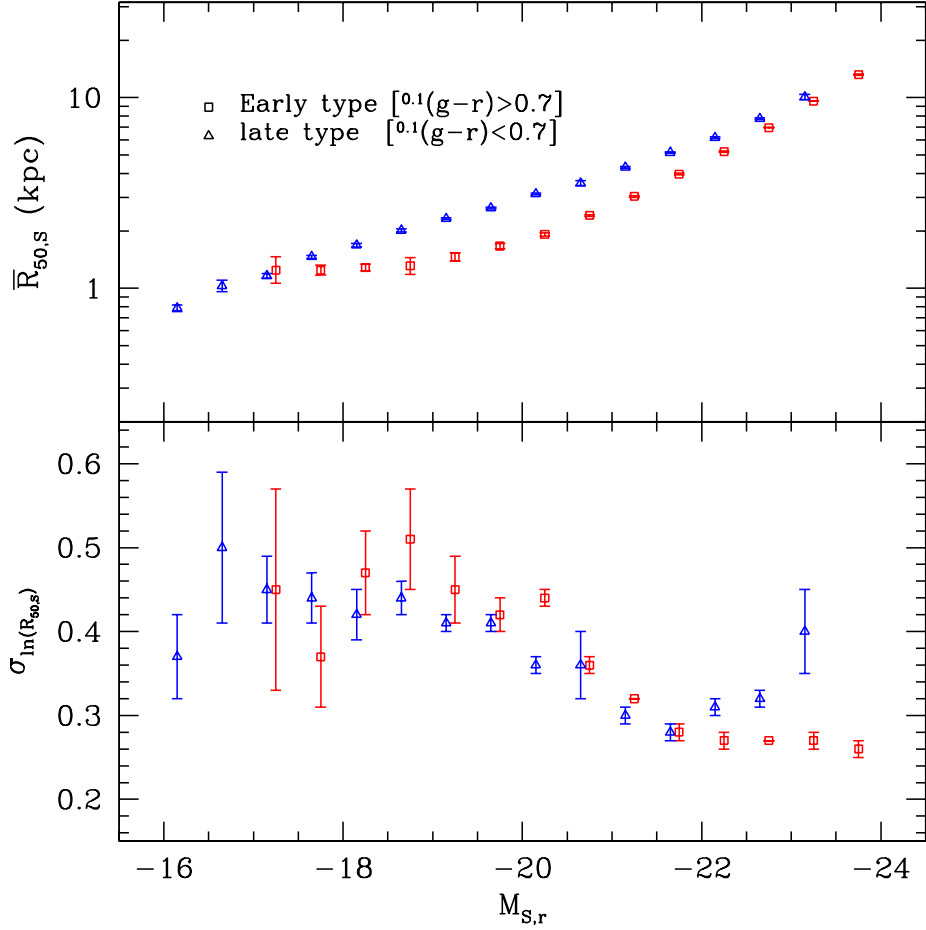
Figure 8. The median and dispersion of the distribution of Sérsic half-light radius $R_{50,S}$, as a function of r-band Sérsic absolute magnitude. Triangles represent results for late-type galaxies [here defined to be those with $^{0.1}(g-r) < 0.7$], while the squares are for early-type galaxies with $^{0.1}(g-r) > 0.7$. The error bars represent the scatter among 20 bootstrap samples.

and the early-type sample ($n > 2.5$) into two equal sub-samples. The ranges of n for these sub-samples and the fitting results are shown in Figure 7. These results should be compared with those shown in Fig. 5. While galaxies with higher n do show a steeper $\bar{R}$ - M relation, the change of the trend with n is less systematic than with c. It seems that galaxies are separated into two groups at $n \sim 1.7$, and galaxies in each group have similar $\bar{R}$ - M relations, independent of n. As shown by the two dimensional distribution of galaxies in the space spanned by n and the $^{0.1}(g-r)$ color (Blanton et al. 2002b), the cut at $n = 1.7$ roughly corresponds to a color cut at $^{0.1}(g-r) \approx 0.7$. The latter cut appears to separate E/S0/Sa from Sb/Sc/Irr galaxies, as discussed in subsection 2.4.

For comparison, we consider separating galaxies according to the color criteria $^{0.1}(g-r) = 0.7$. The results are shown in Figure 8. In this case, since most Sa galaxies are classified as

early-type galaxies, there are fewer bright late-type galaxies. Moreover, we begin to see faint red galaxies (presumably faint ellipticals), which would be classified as 'late-type' galaxies by the c and n criteria, because of their low concentrations. As one can see, the late-type galaxies show approximately the same statistical properties as those in the c and n classifications. This is also true for bright early-type galaxies. Red galaxies with $M_r \sim -20$ seem to follow a parallel trend to late-type galaxies, although they are smaller at given absolute magnitude. This is consistent with the fact that many dwarf ellipticals show exponential surface-brightness profiles, have small sizes, and have size-luminosity scaling relations similar to that of spiral galaxies (e.g. Caon, Capaccioli & D'Onofrio 1993; Kormendy & Bender 1996; Guzman et al. 1997; Prugniel & Simien 1997; Gavazzi et al. 2001). Faint red galaxies with $M_r > -19$ seem to have almost constant size. Note that $\sigma_{\ln R}$ - M show similar dependence on M for both red and blue galaxies.

Since most of the concentrated galaxies have red colors while galaxies with low concentrations can have both blue and red colors, it is interesting to examine the properties of galaxies selected by both color and n. To do this, we consider a case where galaxies with $n < 2.5$ are divided further into two subsamples according to the color criterion $^{0.1}(g - r) = 0.7$. The results are shown in Figure 9. As we can see, B type galaxies (with low n and red color) show a R-M relation which is closer to that of A type (high n) galaxies than that of C-type (blue and low n). Note again that faint red galaxies have sizes almost independent of luminosity. The $\sigma_{\ln R}$ - M relations are similar for all three cases.

So far our discussion has been based on the r-band data. If galaxies possess significant radial color gradients, the size of a galaxy may be different in different wavebands. Furthermore, if galaxies have different colors, the size distribution as a function of luminosity may also be different in different wavebands. To test how significant these effects are, we have analyzed the size distributions separately in the SDSS g, i and z bands, using either the absolute magnitudes in the corresponding band or the absolute magnitudes in the r-band to bin galaxies into luminosity sub-samples. The results are qualitatively the same as derived from the r-band data. Similar conclusions for early type galaxies have been reached by Bernardi et al. (2003b). As an example, we show in Figure 10 the results based on Sérsic radii and Sérsic z-band magnitudes. The galaxies are also separated into late- and early-type by the r-band Sérsic index $n = 2.5$. The results of fitting the $\bar{R}$ - M and $\sigma_{\ln R}$ - M relations are presented in Table 1. Because of the long wavelength involved in the z-band
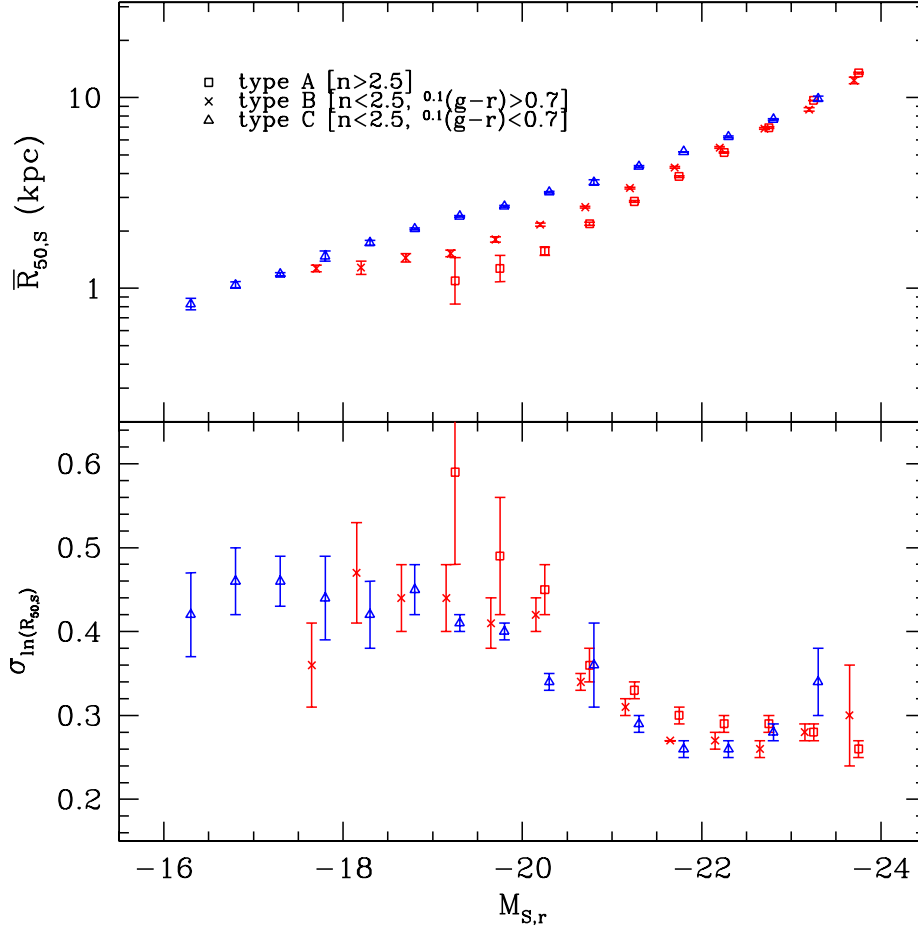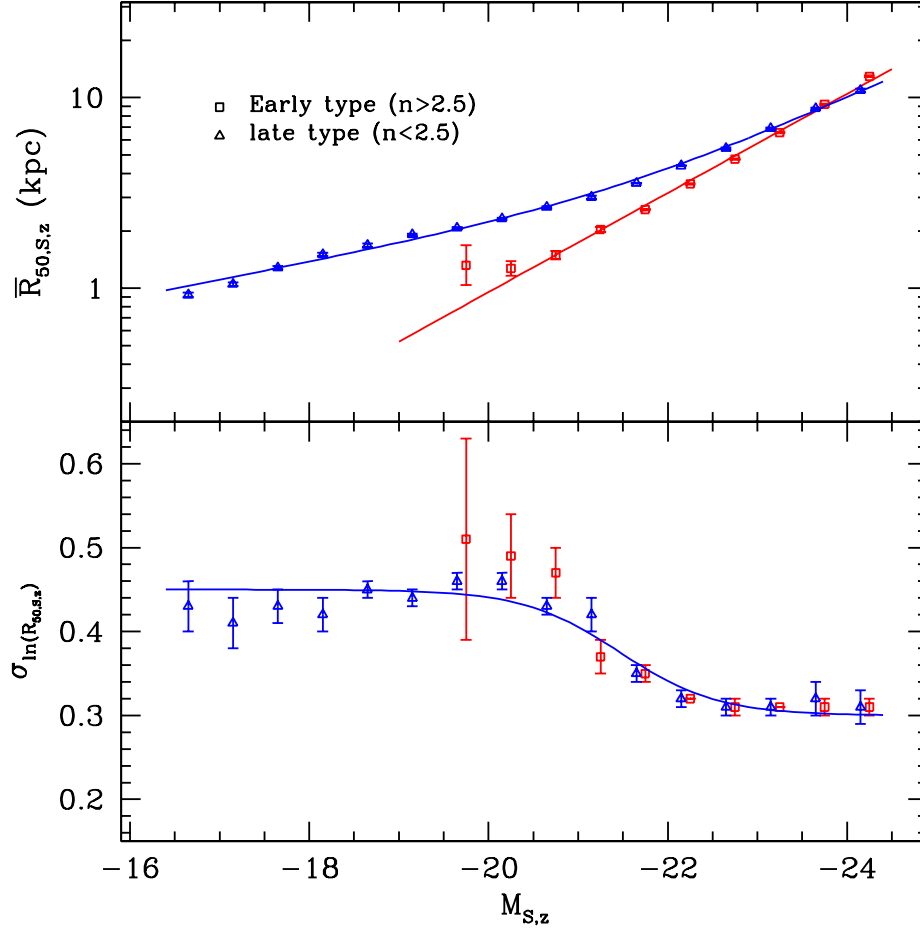
Figure 9. The median and dispersion of the distribution of Sérsic half-light radius $R_{50,S}$ in r-band as a function of r-band absolute Sérsic magnitude. The galaxies are separated into three subsamples according to the Sérsic index n and color $^{0.1}(g-r)$. The error bars represent the scatter among 20 bootstrap samples.

Table 1. The least square fitting results of the parameters in the $\bar{R}$ - M and $\sigma_{\ln R}$ - M relations. Cases of figure 4, 6 and 10 use the fitting formula in equations (14), (15) and (16), while equations (17), (18) and (19) are used for the case of Figure 11.

| | Early type | | Late type | | | | Scatter | |
Case	a	b	α	β	γ	M_0	σ_1	σ_2
Figure 4	0.60	-4.63	0.21	0.53	-1.31	-20.52	0.48	0.25
Figure 6	0.65	-5.06	0.26	0.51	-1.71	-20.91	0.45	0.27
Figure 10	0.65	-5.22	0.23	0.53	-1.53	-21.57	0.45	0.30
Figure 11	0.56	3.47×10^{-5}	0.14	0.39	0.10	3.98×10^{10} M$_\odot$	0.47	0.34

photometry, the quantities in this band may better reflect the properties of the stellar mass (e.g. Kauffmann et al. 2002b).

Figure 10. The median and dispersion of the distribution of Sérsic half-light radius $R_{50,S}$ in the z-band, as a function of z-band Sérsic absolute magnitude. Triangles represent results for late-type galaxies (here defined to be those with $n < 2.5$), while the squares are for early-type galaxies (with $n > 2.5$). The error bars represent the scatter among 20 bootstrap samples. The solid curves are the fit of the $\bar{R}$ - M and $\sigma_{\ln R}$ - M relations by equations (14), (15) and (16).

### 3.3   Size distribution: dependence on stellar mass

In this subsection, we study the size distribution of galaxies as a function of stellar mass. We use the data obtained by Kauffmann et al. (2002a). Figure 11 shows the results based on the z-band Sérsic half-light radii. To quantify the mass dependence of $\bar{R}$ and $\sigma_{\ln R}$, we fit $\bar{R}$ - M relation for the early-type galaxies by

$$\bar{R}(\text{ kpc}) = b \left(\frac{M}{\text{M}_\odot} \right)^a .$$
(17)

For late-type galaxies, we fit $\bar{R}$ - M and $\sigma_{\ln R}$ - M by

$$\bar{R}(\text{ kpc}) = \gamma \left(\frac{M}{\text{M}_\odot} \right)^\alpha \left(1 + \frac{M}{M_0} \right)^{\beta - \alpha}$$
(18)

and
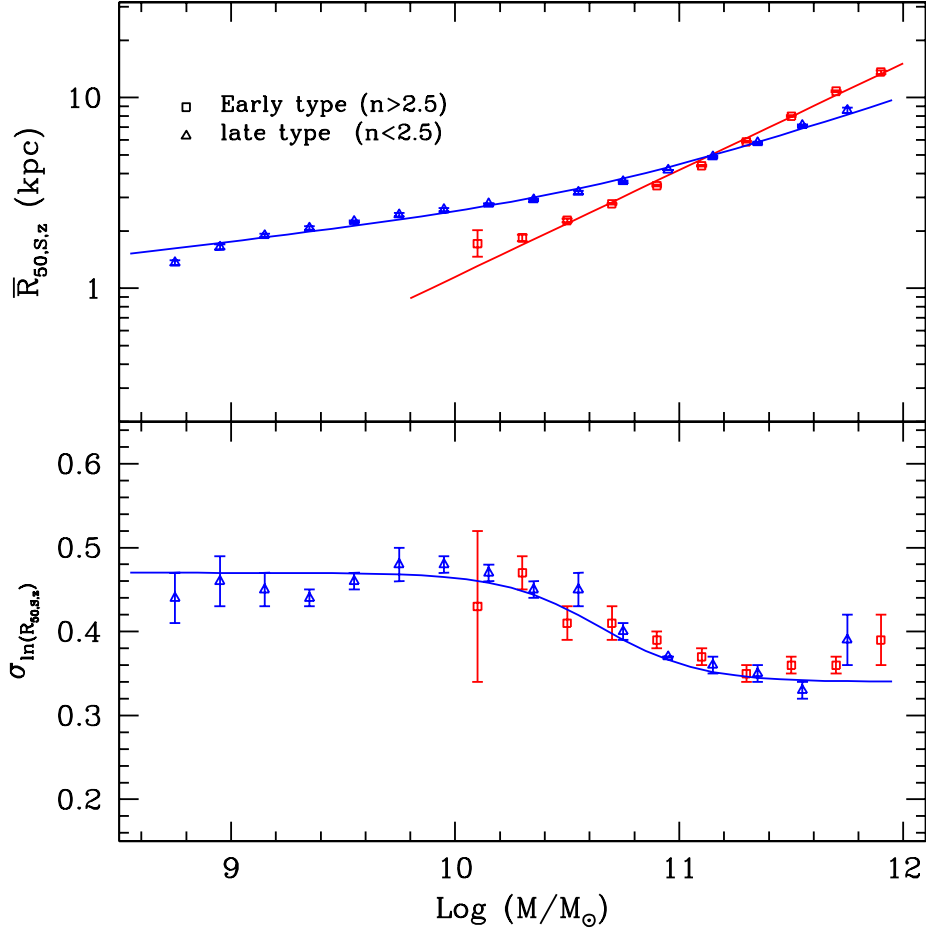
Figure 11. The median and dispersion of the distribution of Sérsic half-light radius $R_{50,S}$ in the z-band, as a function of stellar mass. Triangles represent results for late-type galaxies (here defined to be those with $n < 2.5$), while the squares are for early-type galaxies (with $n > 2.5$). The error bars represent the scatter among 20 bootstrap samples. The solid curves are the fit of the $\bar{R}$ - M and $\sigma_{\ln R}$ - M relations by equations (17), (18) and (19).

$$\sigma_{\ln R} = \sigma_2 + \frac{(\sigma_1 - \sigma_2)}{1 + (M/M_0)^2} \,, \qquad (19)$$

respectively, where M is the stellar mass, α, β, γ, σ_1, σ_2, M_0, a and b are all fitting parameters. Those parameters have the same meaning as those in equations (14), (15) and (16) except that stellar mass is used instead of luminosity. The values of these parameters given by a least square fitting to the data are also listed in Table 1. The fitting results are shown as the solid curves in Fig. 11. Here, similar to the size-luminosity relation, M_0 is the characteristic mass at which $\sigma_{\ln R}$ changes significantly and is about $10^{10.6}$ M$_\odot$. For late type galaxies, the low-mass galaxies ($M \ll M_0$) have $\bar{R} \propto M^{0.14}$ and $\sigma_{\ln R} = 0.47$, and the high-mass galaxies ($M \gg M_0$) have $\bar{R} \propto M^{0.39}$ and $\sigma_{\ln R} = 0.34$. The early type galaxies follow the relation $\bar{R} \propto M^{0.56}$. The power indices a, α and β are smaller for the mass than
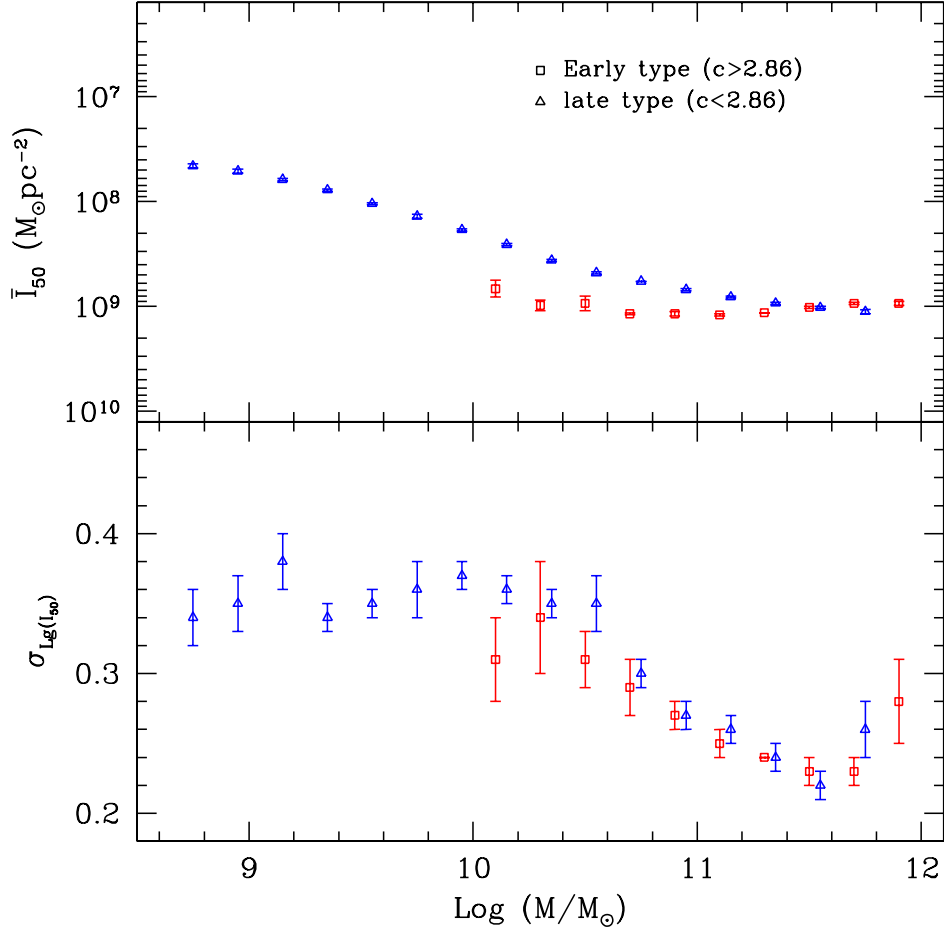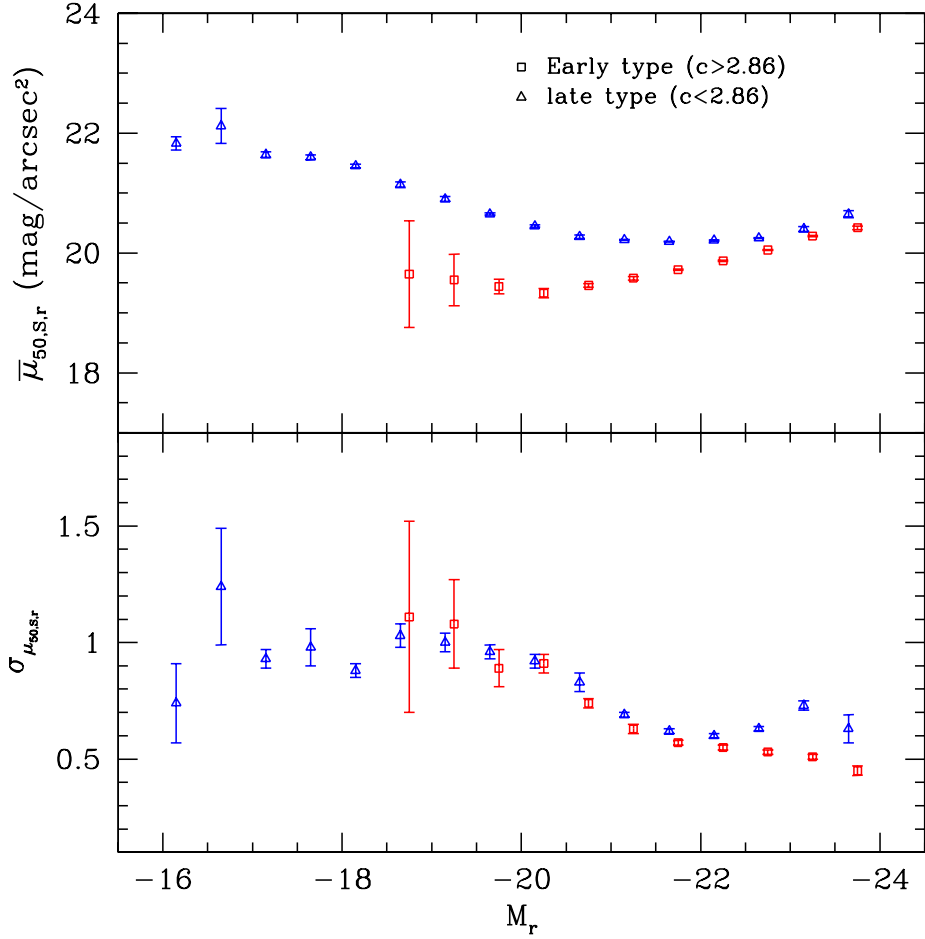
Figure 12. The distributions of the average surface-mass density I_{50} within $R_{50,z}$ as functions of stellar masses. Error bars represent scatter among 20 bootstrap samples.

for the luminosity, because the mass-to-light ratio is systematically higher for galaxies with higher luminosity.

For early-type galaxies, the power index $a = 0.56$ implies that the average surface mass density I_{50} within the half-light radius is roughly a constant, which is shown directly in Fig. 12. Here we have assumed that no mass-to-light ratio gradient exists in the z-band so that the half-light radius also encloses half of the stellar mass. Moreover, since the stellar mass is derived by multiplying the Petrosian luminosity with the model derived mass-to-light ratio M/L (Kauffmann et al., 2002a), the Petrosian half light radius R_{50} is used here in calculating the I_{50}. As we will discuss in Section 5, these results have important implications for the formation of elliptical galaxies.

Figure 13. The median and dispersion of the distribution of r-band effective surface brightness(defined in Sérsic system) as functions of r-band Petrosian absolute magnitude. Triangles represent results for late-type galaxies (here defined to be those with $c < 2.86$), while the squares are for early-type galaxies (with $c > 2.86$). The error bars represent the scatter among 20 bootstrap samples. The two vertical lines denote the observational surface brightness limits (see text).

3.4 The surface-brightness distribution

The intrinsic surface-brightness μ_{50} of a galaxy is linked to its size R_{50} through

$$\mu_{50}(\, \text{magarcsec}^{-2}) = M(\text{mag}) + 5 \, \text{Log} \, R_{50}(\, \text{kpc}) + 38.57, \tag{20}$$

where M represent the absolute magnitude. Thus, the log-normal size distribution for a given luminosity implies that the surface-brightness distribution at a given luminosity is normal. In this case, we may obtain the median and dispersion of the surface-brightness distribution directly from the size distribution through equation (20). However, since the width of our magnitude bins (0.5mag) is finite, the conversion is not accurate. We therefore recalculated the median and dispersion of the surface-brightness distribution in each magnitude bin by using the same maximum-likelihood method as for the size distribution. As an example, we

show the r-band surface-brightness distribution in Figure 13. The surface-brightness used here is defined in the Sérsic system, i.e. the average surface brightness inside the Sérsic half-light radius, but galaxies are labelled by their Petrosian magnitudes. The reason for this is that the luminosity function we are going to use to derive the integrated surface brightness distribution is based on Petrosian magnitudes. As before, galaxies are separated into late- and early-type galaxies at $c = 2.86$. As one can see from Fig. 13, the brighter late-type galaxies have systematically higher surface-brightness while the trend is the opposite for bright early-type galaxies. This is the well-known Kormendy relation (1977). Another feature clearly seen is that the mean value of the surface-brightness is almost independent of luminosity for bright late-type galaxies, which is consistent with the Freeman disk (Freeman 1970). For dwarf late-type galaxies, the surface brightness shows a strong increase with increasing of luminosity in the range $-20 < M_r < -18$. But the median value of the surface brightness is consistent with being constant in the luminosity range $-16 < M_r < -18$. However, this result should be treated with caution, because the median value is already quite close to the limit 23.0 magarcsec^{-2}. Any incompleteness near 23.0 magarcsec^{-2} can bias the median to a lower value (i.e. higher surface brightness).

With the conditional surface-brightness distribution function $f(\mu_{50}|M)$, we can calculate the number density of galaxies at any given surface-brightness μ_{50} by integrating over the luminosity function $\phi(M)$:

$$\phi(\mu_{50}) = \int \phi(M) f(\mu_{50}|M) \, dM \,. \tag{21}$$

The luminosity functions of early- and late-type galaxies separated at $c = 2.86$ have recently been given by Nakamura et al. (2003) based on the Petrosian magnitudes. As shown in Fig. 13, our conditional surface-brightness distribution is reliably determined only in the luminosity range $-24 < M_r < -16$ for late-type galaxies, and in $-24 < M_r < -19$ for early-type galaxies. Therefore, we set the bright end of the integration in equation (21) to be $M_r = -24$ and carry out the integration from a number of low-luminosity limits. The median and dispersion of the surface-brightness distribution at any given magnitude are obtained from a linear interpolation between adjacency magnitude bins. The results are shown on Figure 14 with the faint-end limits labelled on the corresponding curves. The two vertical lines at 18.0 and 23.0 magarcsec^{-2} correspond to the observational surface brightness limits(defined in Petrosian system) of our sample. The bright limit 18.0 magarcsec^{-2} corresponds to the brightest galaxies ($r = 15.0$) with sizes at the lower limit ($1.6''$).
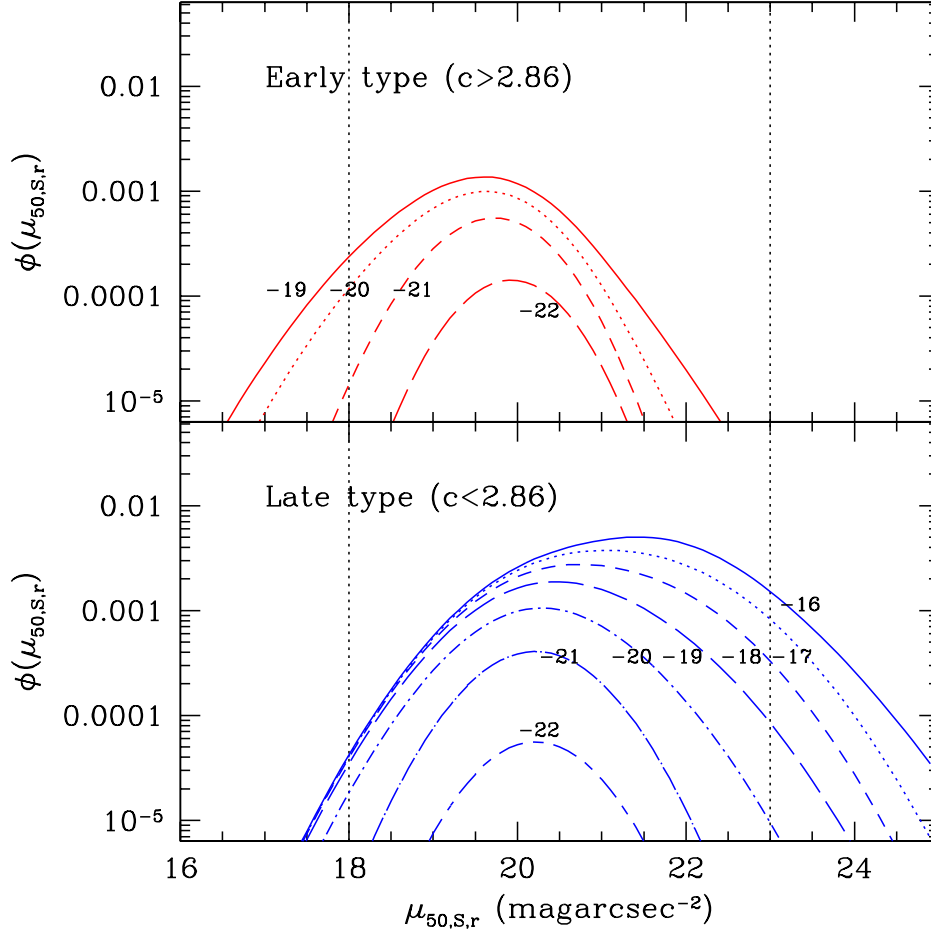
Figure 14. The surface-brightness distribution for late- ($c < 2.86$) and early-type ($c > 2.86$) galaxies in different luminosity ranges, obtained by convolving the observed luminosity function $\phi(L)$ with the conditional surface-brightness distribution $f(\mu_{50}|L)$ shown in Fig. 13.

As one can see from the figure, there may be many compact early-type galaxies that are not included in our sample. For late-type galaxies, the surface-brightness shows a narrow normal distribution for bright galaxies (i.e. the Freeman disk). When more dwarf galaxies are included, low surface-brightness galaxies may contribute a large fraction of the total numbers of galaxies. Unfortunately, the current data cannot give a stringent constraint on the number density of low-surface brightness galaxies because the results for very faint galaxies ($M_r > -16$) are uncertain. However, the fact that galaxies with the lowest surface brightness are predominantly of low luminosity suggests that such low-surface brightness galaxies contribute little to the luminosity density of the universe. A similar conclusion has been reached in earlier analysis (e.g. de Jong & Lacey 2000; Cross & Driver 2002; Blanton et al. 2001).

4   THEORETICAL EXPECTATIONS

In the preceding sections we have seen that the current SDSS data can be used to derive good statistics for the size distribution of galaxies and its dependence on luminosity, stellar mass, concentration and color. In this section, we examine whether or not these observational results can be accommodated in the current paradigm of galaxy formation.

4.1   Late – type galaxies

Let us start with late-type (spiral) galaxies. A spiral galaxy generally consists of a rotationally supported thin disk, and an ellipsoidal bu lge which rotates relatively slowly.

4.1.1   The disk component

According to current theory of galaxy formation, galaxy disks are formed as gas with some initial angular momentum cools and contracts in dark matter haloes. Our model of disk formation follows that described in Mo, Mao & White (1998 hereafter MMW). The model assumes spherical dark haloes with density profile given by Navarro, Frenk & White (1997, hereafter NFW):

$$\rho(r) = \frac{\rho_0}{(r/r_s)(1 + r/r_s)^2},\tag{22}$$

where r_s is a characteristic radius, and ρ_0 is a characteristic density. The halo radius r_{200} is defined so that the mean density within it is 200 times the critical density. It is then easy to show that r_{200} is related to the halo mass M_h by

$$r_{200} = \frac{G^{1/3} M_h^{1/3}}{[10 H(z)]^{2/3}},\tag{23}$$

where $H(z)$ is the is the Hubble constant at redshift z. The total angular momentum of a halo, J, is usually written in terms of the spin parameter,

$$\lambda = J|E|^{1/2} G^{-1} M_h^{-5/2},\tag{24}$$

where E is the total energy of the halo. N-body simulations show that the distribution of halo spin parameter λ is approximately log-normal,

$$p(\lambda)\, d\lambda = \frac{1}{\sqrt{2\pi}\sigma_{\ln\lambda}} \exp\left[-\frac{\ln^2(\lambda/\bar\lambda)}{2\sigma_{\ln\lambda}^2}\right] \frac{d\lambda}{\lambda},\tag{25}$$

with $\bar\lambda \sim 0.04$ and $\sigma_{\ln\lambda} \approx 0.5$ (Warren et al. 1992; Cole & Lacey 1996; Lemson & Kauffmann 1999).

We assume that the disk that forms in a halo has mass M_d related to the halo mass by

$$M_d = m_d M_h \,, \tag{26}$$

and has angular momentum J_d related to the halo spin by

$$J_d = j_d J \,, \tag{27}$$

where m_d and j_d give the fractions of mass and angular-momentum in the disk. Assuming that the disk has an exponential surface density profile and that the dark halo responds to the growth of the disk adiabatically, the disk scale-length R_d can be written as

$$R_d = \frac{1}{\sqrt{2}} \left(\frac{j_d}{m_d} \right) \lambda r_{200} f_r \,, \tag{28}$$

where f_r is a factor that depends both on halo profile and on the action of the disk (see MMW for details). As shown in MMW, for a given halo density profile, f_r depends both on m_d and on $\lambda_d \equiv (j_d/m_d)\lambda$, but the dependence on λ_d is not very strong. Thus, if j_d/m_d is constant, the log-normal distribution of λ will lead to a size distribution which is roughly log-normal.

4.1.2   The bulge component

Our empirical knowledge about the formation of galaxy bulges is still very limited (e.g. Wyse, Gilmore & Franx 1997). Currently there are two competing scenarios in the literature, one is the merging scenario and the other is based on disk instability.

In the merging scenario, galaxy bulges, like elliptical galaxies, are assumed to form through the mergers of two or more galaxies (Toomre & Toomre 1972). Subsequent accretion of cold gas may form a disk around the existing bulge, producing a bulge/disk system like a spiral galaxy (e.g. Kauffmann, White & Guiderdoni 1993; Kauffmann 1996; Baugh, Cole & Frenk 1996; Jablonka, Martin & Arimoto 1996; Gnedin, Norman & Ostriker, 2000). In this scenario, the formation of the bulge is through a violent process prior to the formation of the disk, and so the properties of the bulge component are not expected to be closely correlated with those of the disk that forms subsequently.

In the disk-instability scenario, low-angular momentum material near the centre of a disk is assumed to form a bar due to a global instability; the bar is then transformed into a bulge through a buckling instability (e.g. Kormendy 1989; Norman, Sellwood & Hasan 1996; Mao & Mo 1998; van den Bosch 1998; Noguchi 2000). The first of these instabilities is well documented through direct simulation, the second less so. According to both N-body

simulations (Efstathiou, Lake & Negroponte 1982) and analytic models (e.g. Christodoulou, Shlosman & Tohline 1995) disks may become globally unstable when

$$\epsilon \equiv \frac{V_m}{(GM_d/R_d)^{1/2}} < \epsilon_0 \,, \tag{29}$$

where V_m is the maximum rotation velocity of the disk, and $\epsilon_0 \sim 1$. As discussed in MMW, for a disk in a NFW halo, this criterion can approximately be written as $m_d > \lambda_d$. Thus, for given λ_d, there is a critical value $m_{d,c}$ for m_d above which the disk is unstable. If the overall stellar mass fraction m_g (defined as ratio of total stellar mass to total halo mass) is smaller than $m_{d,c}$, the disk is stable and there is no bulge formation in this scenario. In this case, $m_b = 0$ and $m_d = m_g$. Here, m_b is the bulge fraction, which links the mass of the bulge to the halo mass,

$$M_b = m_b M_h \,. \tag{30}$$

If $m_g > m_{d,c}$, we assume that the bulge mass is such that the disk has $\epsilon = \epsilon_0$, i.e. the disk is marginally unstable. In this case, $m_d = m_{d,c}$ and $m_b = m_g - m_{d,c}$. Note that the gravity of the bulge component must be taken into account when calculating ϵ. To do this, we include a bulge component in the gravitational potential following MMW. For given m_g and λ_d, we then solve for m_b and m_d iteratively.

To proceed further, we assume the angular momentum of the bulge to be negligible. There are two ways in which the bulge may end up with little angular momentum: the first is that it formed from halo material which initially had low specific angular momentum; the second is that the bulge material lost most of its angular momentum to the halo and the disk during formation. In the first case, we assume that the specific angular momentum of the final disk is the same as that of the dark matter, so that $j_d = m_d$. In the second case, the final angular momentum of the disk depends on how much of the bulge's initial angular momentum it absorbs. Numerical simulations by Klypin, Zhao & Somerville (2002) suggest that angular momentum loss is primarily to the disk for bulges that form through bar instability. In general, we assume a fraction of f_J of the bulge angular momentum is transferred to the disk component, and so $J_d = (m_d + f_J m_b)J$. Thus the effective spin parameter for the disk is

$$\lambda_d = \lambda(1 + f_J m_b/m_d) \,, \tag{31}$$

and we use this spin to calculate the disk size.

To complete our description of the disk component, we also need to model the size of the

bulge. Since current models of bulge formation are not yet able to make reliable predictions about the size-mass relation, we have to make some assumptions based on observation. Observed galaxy bulges have many properties similar to those of elliptical galaxies. We therefore consider a model in which galaxy bulges follow the same size-mass relation as early-type galaxies. Specifically, we assume that bulges with masses higher than $2 \times 10^{10}\,\mathrm{M}_{\odot}$ have de Vaucouleurs profiles and have a size-mass relation given by equation (17). For less massive bulges, we adopt exponential profiles and two models for the size-mass relation. In the first model, low-mass bulges follow a size-mass relation which is parallel to that of faint late-type galaxies but has a lower zero point (so that it joins smoothly to the relation for giant ellipticals at $M = 2 \times 10^{10}\,\mathrm{M}_{\odot}$), i.e.

$$\mathrm{Log}\,(R_e/\,\mathrm{kpc}) = \begin{cases} 0.56\,\mathrm{Log}\,(M_b) - 5.54 & \text{for } M_b > 2 \times 10^{10}\,\mathrm{M}_{\odot} \\ 0.14\,\mathrm{Log}\,(M_b) - 1.21 & \text{for } M_b < 2 \times 10^{10}\,\mathrm{M}_{\odot} \end{cases}, \tag{32}$$

where R_e is the effective radius of the bulge. This model is motivated by the fact that dwarf ellipticals obey a size-luminosity relation roughly parallel to that of spiral galaxies (Kormendy & Bender 1996; Guzman et al. 1997; see Figures 7 to 9). In the second model, we assume a size-mass relation which is an extrapolation of that for the massive ellipticals, i.e.

$$\mathrm{Log}\,(R_e/\,\mathrm{kpc}) = 0.56\,\mathrm{Log}\,(M_b) - 5.54\,. \tag{33}$$

In this case, faint bulges are small and compact, like compact ellipticals (Kormendy 1985; Guzman et al. 1997). For simplicity, we do not consider the scatter in the size-mass relation in either case.

With the mass and size known for both the disk and bulge components, we can obtain the surface density profile of the model galaxy by adding up the surface density profiles of the two components:

$$I(r) = I_d(r) + I_b(r)\,, \tag{34}$$

from which one can estimate the half-mass radius for each model galaxy.

4.1.3 The value of m_g

If all the gas in a halo can settle to halo centre to form a galaxy, then $m_g \sim \Omega_{\mathrm{B},0}/\Omega_0$. For the cosmological model adopted here this would imply $m_g \sim 0.13$, much larger than most estimates of the baryon fraction in galaxies. In reality, not all the gas associated with a halo

Table 2. Parameters for the different models itemized in section 4.1.4.

Model	m_0	α	M_c	B/D	f_J	$R_e(M_b)$
I	0.05	0	1×10^{12}	random	0.	eq.(32)
II	0.13	0.67	1×10^{12}	random	0.	eq.(32)
III	0.13	0.67	1×10^{12}	disk instability	1.	eq.(32)
IV	0.13	0.67	1×10^{12}	disk instability	0.	eq.(32)
V	0.13	0.67	1×10^{12}	disk instability	0.5	eq.(32)
VI	0.13	1.	1×10^{12}	disk instability	0.5	eq.(32)
VII	0.13	0.67	1×10^{12}	disk instability	0.5	eq.(33)

may settle into the central galaxy, because feedback from star formation provides a heat source which may expel some of it. Based on such considerations, we consider a feedback model in which the mass fraction m_g in a halo of mass M_h is

$$m_g = \frac{m_0}{1 + (M_h/M_c)^{-\alpha}} \,, \tag{35}$$

where M_c is a characteristic mass, α is a positive index, and m_0 is a constant representing the mass fraction in systems with $M_h \gg M_c$ (e.g. White & Frenk 1991). We set $m_0 = \Omega_{B,0}/\Omega_0 = 0.13$, so that m_g is suppressed for small haloes. Galaxy wind models suggest that the circular velocity corresponding to M_c is about $150\,\mathrm{km\,s^{-1}}$, i.e. $M_c \sim 10^{12}\,\mathrm{M_\odot}$, and the value of α is 2/3. If the intergalactic medium is preheated to a high entropy, then α is about 1 (Mo & Mao 2002).

4.1.4 Specific models

To summarize, there are four key ingredients in the scenarios described above. The first is the feedback process which gives the mass fraction m_g. We use the parameterized form given in equation (35) to model this process, and the model parameters are m_0, α and M_c. The second is the bulge/disk ratio B/D. This ratio is assumed to be either uniform on the interval $[0, 1]$ or given by the instability criterion. The third is the amount of angular momentum transfer between bulge and disk components, as characterized by the parameter f_J in equation (31). The fourth is the size-mass relation of small bulges characterized by equation (32) or (33).

To consider these different possibilities, we have chosen seven models as illustrations. In the following we summarize these models in some detail; their parameters are listed in Table 2.

• **Model I**: Here the mass fraction is chosen to be a constant $m_g = 0.05$, in contrast to the feedback model where m_g changes with halo mass, and the B/D ratio is assumed to be random in the interval $[0, 1]$. Disks are generated according to the model described

in subsection 4.1.1, and bulges are assigned sizes according to equation (32). No angular-momentum transfer from the bulge component to the disk is assumed.

- **Model II**: Here m_g is assumed to follow equation (35), with $m_0 = 0.13$, $\alpha = 2/3$, and $M_c = 10^{12}\,\mathrm{M_\odot}$. Other assumptions are the same as Model I.

- **Model III**: In this model m_g is assumed to follow equation (35), with $m_0 = 0.13$, $\alpha = 2/3$, and $M_c = 10^{12}\,\mathrm{M_\odot}$. Bulges are generated based on disk instability. All of the initial angular momentum of the bulge is assumed to be transferred to the disk, i.e. $f_J = 1$. The size-mass relation of the bulge component follows equation (32).

- **Model IV**: This model is the same as Model III, except that there is no angular momentum transfer, i.e. $f_J = 0$.

- **Model V**: This model is also the same as Model III, except that half of the initial angular momentum of the bulge material is transferred into the disk (i.e. $f_J = 0.5$).

- **Model VI**: This model is the same as Model V, except that α is assumed to be 1 instead of 2/3.

- **Model VII**: This model is the same as Model V, except that the size-mass relation of bulge is equation (33) instead of Eq. (32)

4.1.5 Model predictions

We use Monte-Carlo simulations to generate galaxy samples for each of the models described above. To do this, we first use the Press-Schechter (1974) formalism to generate 50,000 dark matter haloes at redshift zero with masses (parameterized by circular velocity V_c) in the range $35\,\mathrm{km\,s^{-1}} < V_c < 350\,\mathrm{km\,s^{-1}}$ and with a log-normal spin parameter distribution with $\bar{\lambda} = 0.03$ and $\sigma_{\ln \lambda} = 0.45$ (see equation 25).

We then use equations (23) – (35) to calculate the sizes and masses of the disk and bulge for each galaxy. Finally, we combine the disk and bulge of each galaxy to calculate its half-mass radius. As for the observational data, we sort galaxies into stellar mass bins and calculate the median and dispersion of the size distribution as functions of stellar mass.

Figure 15 compares results for the seven models with the observational data for the z-band Sérsic half-light radii of late-type galaxies ($n < 2.5$) as function of stellar masses. As one can see, if m_g is assumed to be a constant, (Model I), the predicted median size-mass relation is $\bar{R} \propto M^{1/3}$, which is completely inconsistent with observations of low mass galaxies. The predicted $\sigma_{\ln R}$ is also too large. When m_g is assumed to change with halo mass
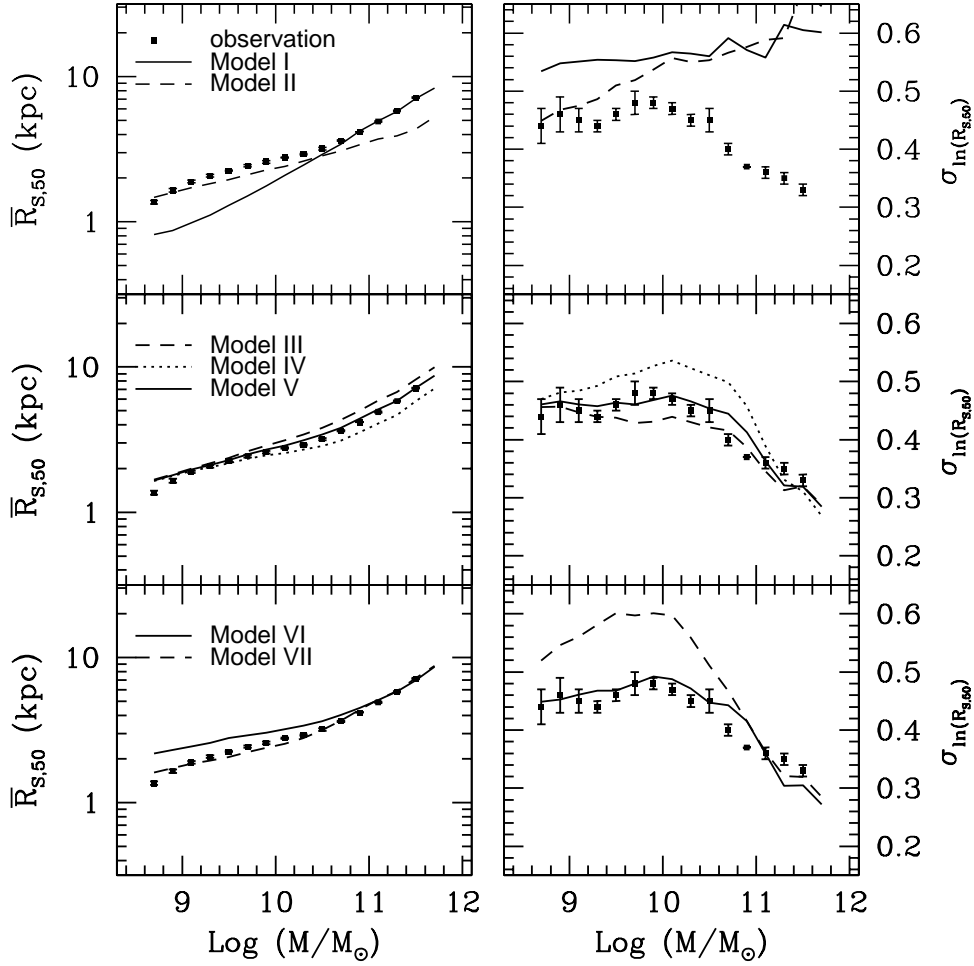
Figure 15. The median and dispersion of the distribution of half-mass radius of spiral galaxies predicted by different models in comparison with the observed distribution of the z-band Sérsic half-light radius as function of stellar mass (Fig. 11). Observational results are shown only for galaxies with $n < 2.5$. The models are described in detail in section 4.1.4 and model parameters are listed in Table 2.

as suggested by the feedback scenario (Model II), the predicted shape of $\bar{R}$ - M is similar to that observed for low mass galaxies, but the predicted median sizes are too small for high mass galaxies. The predicted dispersion is also too big for high mass galaxies. If bulges are assumed to form through disk instability and if $f_J = 1$ (Model III), the predicted scatter follows the observations, but the predicted median sizes are too big for massive galaxies. On the other hand, if no angular momentum is transferred, i.e. $f_J = 0$ (Model IV), the predicted median size is smaller at the high mass end and the predicted scatter becomes systematically higher. To match the observed behavior of the median and the dispersion simultaneously, $f_J \sim 0.5$ seems to be required (Model V). Changing the value of α from 2/3 to 1 (Model VI) gives a median size which is slightly too high for low-mass galaxies. If the
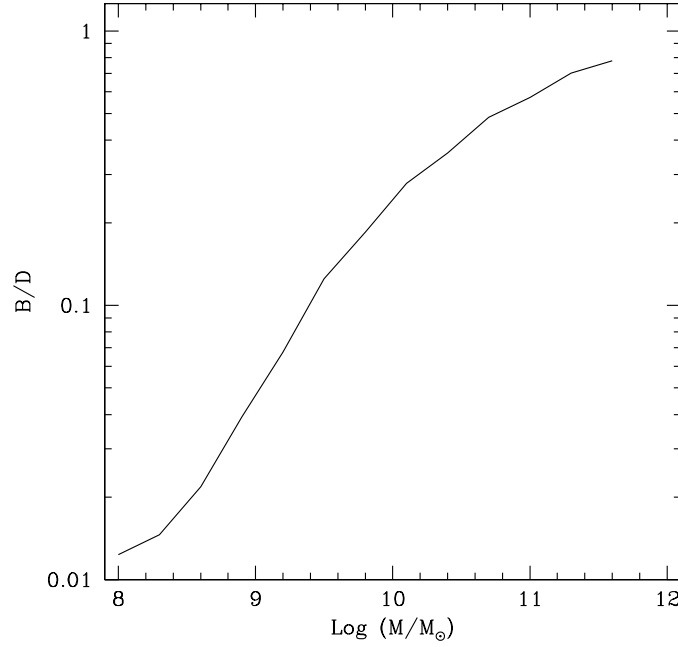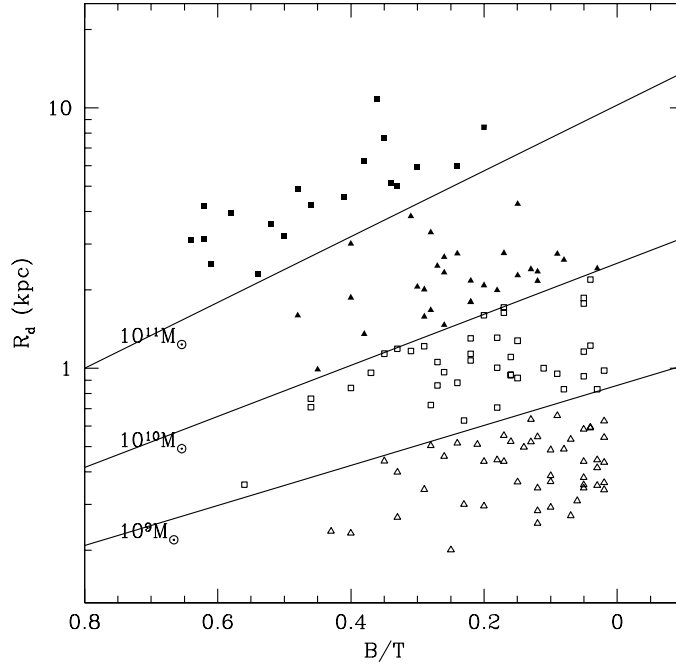
Figure 16. The prediction of Model V for the average bulge/disk ratios for galaxies with different stellar masses.

size-mass relation for small bulges is assumed to be an extension of that for big ellipticals (Model VII), higher scatter is predicted for low mass galaxies.

Given that Model V reproduces the observed $\bar{R}$ - M and $\sigma_{\ln R}$ - M relations, it is interesting to look at other predictions of the model. In this case, the bulge/disk ratio depends on the mass of the halo. A larger halo mass gives a larger value of m_g and, in the disk-instability model, this implies a larger bulge fraction. Hence we expect B/D to increase with galaxy mass. Figure 16 shows the mean B/D ratio as a function of M according to Model V. The predicted trend is consistent with the observed correlation between B/D and galaxy mass (e.g. Roberts & Haynes 1994).

The formation of the bulge depends on the properties of the disk in the disk-instability-driven scenario. The bulge fraction ($B/T \equiv m_b/m_g$) should therefore be correlated with disk size. In Figure 17, we show disk size as a function of B/T for a number of randomly selected Model V galaxies. The points of different type represent galaxies of differing stellar masses; open triangles, open squares, solid triangles and solid squares represent galaxies with masses from 10^8 M$_\odot$ to 10^{11} M$_\odot$ respectively. The rough separation of galaxies according to mass is delineated by the solid lines in the figure. On average, galaxies with larger B/T ratios have larger disks. This is mainly due to the positive correlation between B/T and galaxy mass.

Figure 17. The prediction of Model V for the relation between disk scale-length and bulge/total mass ratio for late-type galaxies. The points with different symbols represent galaxies in different mass ranges (as shown by the solid lines).

For a given stellar mass, galaxies with large B/T ratios have smaller disks. This is consistent with the observational results of de Jong (1996). If the bulge/disk ratio is assumed to be random, as in Models I and II, disk size is independent of B/T.

4.2   Early-type galaxies

Currently the most appealing model for the formation of elliptical galaxies assumes they result from the merging of smaller systems. Numerical simulations have shown that mergers of disk galaxies of similar mass do indeed produce remnants resembling elliptical galaxies (e.g. Negroponte & White 1983; Hernquist 1992). However, it seems unlikely that every elliptical is the remnant of a merger between two similar spirals drawn from the observed local population. On the one hand, the stellar population of early-type galaxies is found to be so old that the typical star formation epoch must be at $z > 2$ (e.g. Bernardi et al. 1998, 2003d; Thomas, Maraston & Bender 2002). On the other hand, detailed modelling of the merger histories of galaxies in a CDM universe suggests that each elliptical obtains its stars from progenitors covering a wide range in stellar mass, that the effective number of progenitors increases weakly with the mass of the elliptical, that the last major merging event is typically around redshift unity but with a wide dispersion, and that the progenitors may
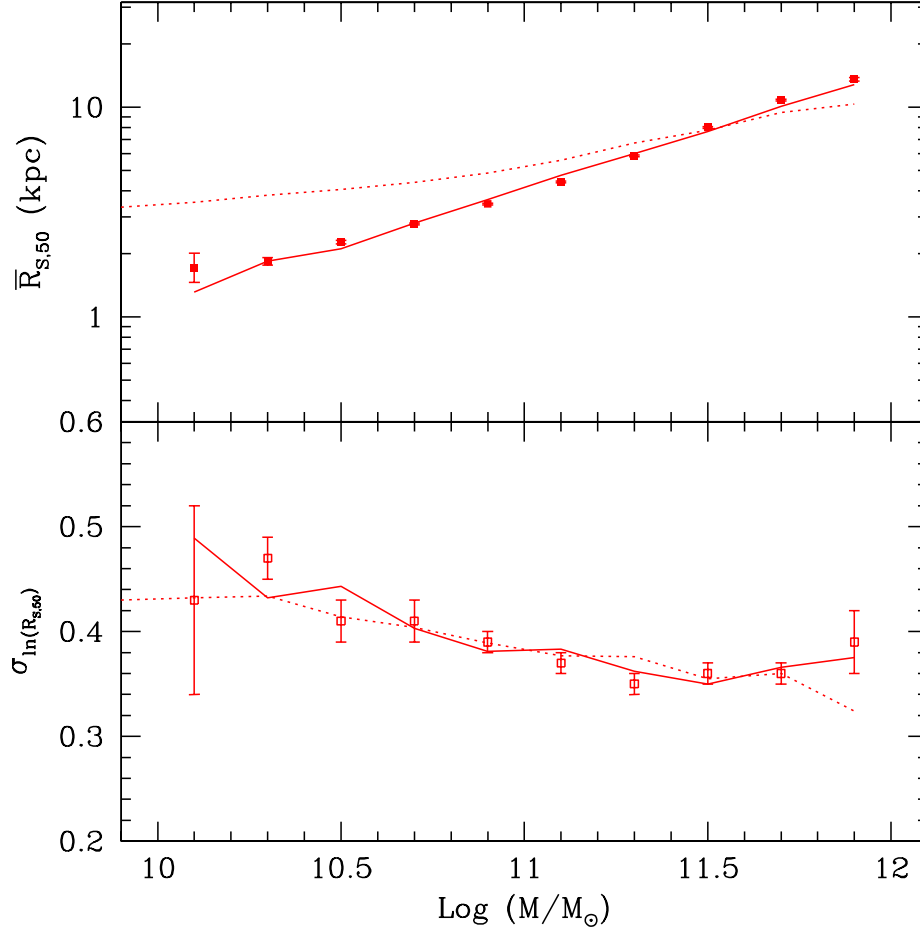
Figure 18. Model predictions for the size distribution of early type galaxies. The solid lines assume ellipticals to be built by repeated merging from a population of small progenitors, while the dotted lines show a model where each elliptical forms from the merger of two similar, late type galaxies. The observed size distribution of early type galaxies ($n > 2.5$) is reproduced from Fig. 11 for comparison.

have been gas-rich, producing a substantial fraction of the observed stars during merger events (Kauffmann 1996; Baugh et al. 1996; Kauffmann & Charlot 1998; Kauffmann & Haehnelt 2000). Rather than treating the detailed merger statistics of CDM models, we here contrast two simpler models, one where ellipticals are built up by random mergers within a pool of initially small progenitors, the other where they form through a single merger of a pair of similar "spirals". As we will see, these pictures predict rather different size-mass relations for the resulting population. Consider two galaxies with stellar masses M_1 and M_2, and corresponding half-mass radii R_1 and R_2, which merge to form a new galaxy with stellar mass M and size R. If we assume that all of the stars end up in the remnant, then $M = M_1 + M_2$. This is an approximation, because numerical simulations show that a

small amount of mass typically becomes unbound as a result of violent potential fluctuations during merging. On dimensional grounds we can write the total binding energy of the stars in each progenitor as $E_i = -C_i G M_i^2 / R_i$ $(i = 1, 2)$, where C_i depends on the density structure of the galaxy in consideration. In the absence of dark matter, $C_i \approx 0.25$ for an exponential disk, while for a Hernquist (1990) profile (for which the projected profile approximates the $R^{1/4}$ law), $C_i \approx 0.2$. If we assume that the two progenitors and the merger remnant all have similar structure, we can write

$$\frac{M^2}{R} = \frac{M_1^2}{R_1} + \frac{M_2^2}{R_2} + f_{\mathrm{orb}} \frac{M_1 M_2}{R_1 + R_2}, \tag{36}$$

where f_{orb} is a parameter which encodes the amount of energy transferred from the stellar components of the two galaxies to the surrounding dark matter as they spiral together. The form of this term is a simple model suggested by the expected asymptotic scalings (see Cole et al. 2000) but unfortunately the appropriate value of f_{orb} depends both on the structure of the galaxies and their haloes and on the details of the merging process. If we assume the galaxies to have no dark haloes and to merge from a parabolic orbit, then $f_{\mathrm{orb}} = 0$. If the two progenitors are identical then in this case $M = 2M_1$ and $R = 2R_1$. It is easy to see that $R \propto M$ also for repeated mergers with these assumptions. Since our SDSS results imply $R \propto M^{0.56}$, this simple model can be ruled out.

In order for two galaxies with the same mass $(M_1 = M_2)$ and radius $(R_1 = R_2)$ to merge to form a new galaxy with mass $M = 2M_1$ and radius $R = 2^{0.56} R_1$, equation (36) requires $f_{\mathrm{orb}} \approx 1.5$. If we assume f_{orb} remains constant at this value and repeat the binary merging p times, each using remnant from the previous time, then the mass and size of the remnants will grow as $M = 2^p M_1$ and $R = 2^{0.56p} R_1$. Then $R \propto M^{0.56}$, reproducing the observed relation. Motivated by this, we consider a model in which a giant elliptical is produced by a series of mergers of small galaxies. We note that the observed masses ($\sim 10^{10}$ $M_\odot$) and half-mass radii ($\sim 1h^{-1}$ kpc) of faint early-type galaxies (see Fig. 11) are similar to the masses and half-mass radii of Lyman-break galaxies observed at $z \sim 3$ (Giavalisco, Steidel & Macchetto 1996; Lowenthal et al. 1997; Pettini et al. 2001; Shu, Mao & Mo 2001). These may perhaps be suitable progenitors. We assume the progenitor population to have masses $\sim 10^{10}$ $M_\odot$ and sizes given by a log-normal distribution with $\bar{R} = 1.3$ kpc and $\sigma_{\ln R} = 0.5$ (as observed for faint ellipticals). We first use a Monte-Carlo method to generate 100,000 progenitors. We randomly select two galaxies from the progenitor pool and merge them to form a new galaxy according to equation (36). After returning the new galaxy to the pool

and deleting its progenitors, we repeat this procedure many times. Based on the discussion above, we assume $f_{\rm orb}$ to be normally distributed with mean $\bar{f} = 1.5$ and a dispersion σ_f to be specified. After 90,000 mergers, we obtain 10,000 galaxies with a broad distribution of mass and radius. For this sample we use the maximum likelihood method described in Section 3 to estimate the median and dispersion of the size distribution as functions of stellar mass. The value of σ_f is tuned to 1.35 so that the predicted $\sigma_{\ln R}$ matches the observations for the most massive galaxies. The model predictions so obtained are shown in Fig. 18 as the solid curves, together with the observational results. This simple model nicely reproduces the observed size distribution for early-type galaxies.

For comparison, we have considered another model in which early-type galaxies are produced by a single major merger between two present-day spirals. We define a major merger to be one where the mass ratio of the progenitors is larger than $1/3$. We use the observed late-type galaxy population as progenitors, and randomly merge two of them to form an early-type galaxy with size given by equation (36). Here again $f_{\rm orb}$ is assumed to have a normal distribution with mean 1.5 and dispersion 1.35. The results for $\bar{R}$ - M and $\sigma_{\ln R}$ - M are shown as the dotted lines in Fig. 18. In this case, $\bar{R}$ is predicted to scale with M in the same way as for the progenitors. This conflicts with the observational results for early-type galaxies. A possible resolution may be that typical merger epochs are later for more massive systems. Since disk galaxies are predicted to be larger and lower density at later times (e.g. MMW; Mao, Mo & White 1998) this results in a steepening of the predicted dependence of R on M. From the scaling laws of MMW it easy to show that the typical cosmic time at which merging occurs has to increase with elliptical mass roughly as $t \propto M^{0.4}$ to reproduce the observed scaling of size with mass. This slow dependence is perhaps compatible with the expected dependence of formation time on halo mass in hierarchical cosmologies (Lacey & Cole 1993).

5 DISCUSSION AND SUMMARY

In this paper, we use a sample of $140,000$ galaxies from the SDSS to study the size distribution of galaxies and its dependence on the luminosity, stellar mass and morphological type of galaxies. This database provides statistics of unprecedented accuracy. These confirm a number of previously known trends, for example, the approximately constant surface brightness of luminous late-type galaxies (the "Freeman disk"), the Kormendy relations be-

tween surface brightness and luminosity for ellipticals, and a roughly log-normal form for the size distribution function at fixed luminosity. We are able to quantify these properties, and to show other relations that cannot be seen in smaller samples. We find that, for late-type galaxies, there is a characteristic luminosity at $M_{r,0} \sim -20.5$ (assuming $h = 0.7$) corresponding to a stellar mass $M_0 \sim 10^{10.6}$ $M_\odot$. Galaxies more massive than M_0 have median size $\bar{R} \propto M^{0.4}$ and have dispersion in the size distribution $\sigma_{\ln R} \sim 0.3$. For less massive galaxies, $\bar{R} \propto M^{0.15}$ and $\sigma_{\ln R} \sim 0.5$. The $\bar{R}$ - M relation is significantly steeper for early-type galaxies, with $\bar{R} \propto M^{0.55}$, but the $\sigma_{\ln R}$ - M relation is similar to that of late-type galaxies. Fainter than $M_r \sim -20$ the properties of red galaxies are not a simple extrapolation of the relations for bright early-type systems. These faint galaxies have low concentrations and their half-light radii are almost independent of luminosity. Brighter than $M_r \sim -20$ the mean surface brightness of early-type galaxies also declines, so that systems near $M_r = -20$ have the highest values. In contrast, the average surface *mass* densities of early-type galaxies are independent of luminosity above $M_r \sim -20$.

We use simple theoretical models to understand the implications of our observational results for galaxy formation. We find that the observed $\bar{R}$ - M relation for late-type galaxies can be explained if the material in a galaxy has specific angular momentum similar to that of its halo, and if the fraction of baryons that form stars is similar to that in standard feedback models based on galactic winds. A successful model for the observed $\sigma_{\ln R}$ - M relation also requires the bulge/disk mass ratio to be larger in haloes of lower angular momentum and the bulge material to transfer part of its angular momentum to the disk component. We show that this can be achieved if the amount of material that forms a galactic bulge is such that the disk component is marginally stable.

For early-type galaxies, the observed $\sigma_{\ln R}$ - M relation is inconsistent with the assumption that they are the remnants of major mergers of present-day disks. It may be consistent with a model where the major mergers which formed lower mass ellipticals occurred at earlier times and so involved more compact disks. The observed relation is consistent with a model where early-type galaxies are the remnants of repeated mergers, provided that the progenitors have properties similar to those of faint ellipticals and that the orbital binding energy is significant when two galaxies merge.

A number of issues remain unresolved in the present study. First, the photometric errors of the half-light radii are not considered in our analysis, which would finally convolved in the derived dispersions of the size distribution. Unfortunately, an accurate assessment of error

is difficult to make. To test how significant this effect can be, we have done Monte-carlo simulations including artificial errors in the measurements of the sizes. We found that if the measurement errors are less than 10 percent (assuming a Gaussian distribution), the effect on the derived width of size distribution is negligible. Another uncertainty is connected to the fact that our galaxy sample covers a non-negligible range in redshift while galaxy sizes are based on half light radii in a fixed band in the *observational* frame rather than in a fixed band in the rest frame. However, this effect should be quite weak because the sizes of galaxies are quite independent of the wavelength as we have found (see also Bernardi et al. 2003b). Yet another uncertainty may be caused by luminosity evolution of galaxies, which may affect the derived $R - L$ relation (see e.g. Schade et al. 1996, 1997; Bernardi et al. 2003b). This effect should not be large in our results, since most of our galaxies are located in a relatively narrow redshift range ($0.05 < z < 0.15$). As a check, we have analyzed a sample which only includes galaxies with redshift $z < 0.1$ and found negligible change in any of our results. Finally, since faint ellipticals have light profiles similar to those of disc galaxies, type classifications based on concentrations and profile indices miss these objects. Classifying according to color suggests that these galaxies may have properties different both from massive early-type galaxies and from spiral galaxies, but it is unclear if all faint red galaxies in our samples are ellipticals. To resolve this issue, we need a more accurate indicator of morphological type. One way forward is to carry out disk/bulge decompositions for a large number of galaxies. Such work is underway in the SDSS Collaboration. With such decompositions, we can study the properties of the disk and bulge components separately, and so answer questions such as whether bulges have similar properties to elliptical galaxies of the same luminosity.

the Institute for Advanced Study, the Japan Participation Group, The Johns Hopkins University, Los Alamos National Laboratory, the Max-Planck-Institute for Astronomy (MPIA), the Max-Planck-Institute for Astrophysics (MPA), New Mexico State University, University of Pittsburgh, Princeton University, the United States Naval Observatory, and the University of Washington.

REFERENCES

Andredakis Y.C., Peletier R.F., Balcells M., 1995, MNRAS, 275, 874

Baugh C.M., Cole S., Frenk C.S., 1996, MNRAS, 283, 1361

Bernardi M., Renzini A., da Costa L.N., Wegner G., Alonso M.V., Pellegrini P.S., Rit C., Willmer C.N.A., 1998, ApJ, 536, 571

Bernardi M. et al., 2003a, AJ accepted (astro-ph/0301631)

Bernardi M. et al., 2003b, AJ accepted (astro-ph/0301624)

Bernardi M. et al., 2003c, AJ accepted (astro-ph/0301626)

Bernardi M. et al., 2003d, AJ accepted (astro-ph/0301629)

Blanton M.R. et al., 2001, AJ, 121, 2358

Blanton M.R., Brinkmann J., Csabai I., Doi M., Eisenstein D., Fukugita J., Gunn J.E., Hogg D.W., Schlegel D.J., 2002a, AJ submitted (astro-ph/0205243)

Blanton M.R. et al., 2002b, ApJ, submitted (astro-ph/0209479)

Blanton M.R. et al., 2002c, ApJ, submitted (astro-ph/0210215)

Blanton M.R., Lupton R.H., Maley F.M., Young N., Zehavi I., Loveday J., 2003, 125, 2276

Caon N., Capaccioli M., D'Onofrio M., 1993, MNRAS, 265, 1013

Choloniewski J., 1985, MNRAS, 214, 197

Chritodoulou D.M., Shlosman I., Tohline J.E., 1995, ApJ, 443, 551

Cole S., Lacey C.G., 1996, MNRAS, 281, 716

Cole S., Lacey C.G., Baugh C.M., Frenk C.S., 2000, MNRAS, 319, 168

Cross N., Driver S.P., 2002, MNRAS, 329, 579

de Jong R., 1996, A&A, 313, 45

de Jong R., Lacey C., 2000, ApJ, 545, 781

Dressler A., 1980, ApJ, 236, 351

Dressler A., Lynden-Bell D., Burstein D., Davies R.L., Faber S.M., Terlevich R.J., Wegner G., 1987, ApJ, 313, 42

Dressler A., Oemler A.J., Couch W.J., Smail I., Ellis R.S., Barger A., Butcher H., Poggianti B.M., Sharples R.M., 1997, ApJ, 490, 577

Eisenstein D.J. et al., 2001, AJ, 122, 2267

Efstathiou G., Lake G., Negroponte J., 1992, MNRAS, 258, 1

Folkes S. et al., 1999, MNRAS, 308, 459

Freeman K.C. 1970, ApJ, 160, 811

Fukugita M., Ichikawa T., Gunn J.E., Doi M., Shimasaku K., Schneider D.P., 1996, AJ, 111, 1748

Gavazzi G., Zibetti S., Boselli A., Franzetti P., Scodeggio M., Martocchi S., 2001, A&A, 372, 29

Giavalisco M., Steidel C.C., Macchetto F.D., 1996, ApJ, 470, 189

Gnedin N.Y., Norman M.L., Ostriker J.P., 2000, ApJ, 540, 32

Gunn J.E., Carr M.A., Rockosi C.M., Sekiguchi M. et al., 1998, AJ, 116, 3040

Guzman R., Gallego J., Koo D.C., Phillips A.C., Lowenthal J.D., Faber S. M., Illingworth G.D., Vogt N.P., 1997, ApJ, 489, 559

Hernquist L., 1990, ApJ, 356, 359

Hernquist L., 1992, ApJ, 400, 460

Hogg D.W., Finkbeiner D.P., Schlegel D.J., Gunn J.E., 2001, AJ, 122, 2129

Jablonka P., Martin P., Arimoto N., 1996, AJ, 112, 1415

Kauffmann G., White S.D.M., Guiderdoni, B., 1993, MNRAS, 264, 201

Kauffmann G., 1996, MNRAS, 281, 487

Kauffmann G., Charlot S., 1998, MNRAS, 294, 705

Kauffmann G., Haehnelt M., 2000, MNRAS, 311, 576

Kauffmann G. et al., 2002a, MNRAS, in press (astro-ph/0204055)

Kauffmann G. et al., 2002b, MNRAS, in press (astro-ph/0205070)

Klypin A., Zhao H., Somerville R.S., 2002, ApJ, 573, 597

Kormendy J., 1977, ApJ, 217, 406

Kormendy J., 1985, ApJ, 295, 73

Kormendy J., 1989, ApJ, 342, 63

Kormendy J., Bender R., 1996, ApJ, 464, 119

Lacey C., Cole S., 1993, MNRAS, 262, 627

Lemson G., Kauffmann G., 1999, MNRAS, 302, 111

Lin H., Kirshner R.P., Shectman S.A., Landy S.D., Oemler A., Tucker D.L., Schechter P.L., 1996, ApJ, 464, L60

Loveday J., Peterson B.A., Efstathiou G., Maddox S.J., 1992, ApJ, 390, 338

Lowenthal J.D., Koo D.C., Guzman R., Gallego J., Phillips A.C., Faber S.M., Vogt N.P., Illingworth G.D., Gronwall C., 1997, ApJ, 481, 673

Lupton R.H., Gunn J. E., Ivezic Z., Knapp G.R., Kent S., Yasuda N., 2001, ADASS X. ed. F.R. Harnden, Jr., F.A. Primini, & H.E. Payne, ASP Conf Proc 238, 269.

Lupton R.H., Gunn J. E., Ivezic Z., Knapp G.R., Strauss M., Yasuda N., 2002, Proc. SPIE, in press

Madgwick D.S. et al., 2002, MNRAS, 333, 133

Mao S., Mo H.J., 1998 (astro-ph/9805094)

Mao S., Mo H.J., White S.D.M., 1998, MNRAS, 297, L71

Mo H.J., Mao S., White S.D.M., 1998, MNRAS, 295, 319 (MMW)

Mo H.J., Mao S., 2002, MNRAS, 333, 768

Nakamura O., Fukugita M., Yasuda N., Loveday J., Brinkmann J., Schneider D.P., Shimasaku K., SubbaRao M., 2003, AJ, 125, 1682

Navarro J., Frenk C.S., White S.D.M., 1997, ApJ, 49, 493 (NFW)

Negroponte J., White S.D.M., 1983, MNRAS, 205, 1009

Noguchi M., 2000, MNRAS, 312, 194

Norman C.A., Sellwood J.A., Hasan H., 1996, ApJ, 462, 114

Petrosian V., 1976, ApJ, 209, L1

Pettini M., Shapley A.E., Steidel C.C., Cuby J.G., Dickinson M., Moorwood A.F.M., Adelberger K.L., Giavalisco M., 2001, ApJ, 554, 981

Pier J.R., Munn J.A., Hindsley R.B., Hennessy G.S., Kent S.M., Lupton R.H., Ivezic Z., 2003, AJ, 125, 1559

Press W.H., Schechter P., 1974, ApJ, 187, 425

Prugniel P., Simien F., 1997, A&A, 321, 111

Roberts M.S., Haynes M.P., 1994, ARA&A, 32, 115

Schade D., Carlberg R.G., Yee H.K.C., Lopez-Cruz, O., Ellingson E., 1996, ApJ, 464, L63

Schade D., Barrientos L.F., Lopez-Cruz O., 1997, ApJ, 477, L17

Schlegel D.J., Finkbeiner D.P., Davis M., 1998, ApJ, 500, 525

Schmidt M., 1968, ApJ, 151, 393

Sérsic J. L., 1968, Atlas de Galaxies Australes (Cordoba: Obs. Astronomico)

Sheth R.K. et al., 2003, ApJ submitted (astro-ph/0303092)

Shimasaku K. et al., 2001, AJ, 122, 1238

Shu C., Mao S., Mo H.J., 2001, MNRAS, 327, 895

Smith J.A., Tucker D.L, Kent S.M. et al., 2002, AJ, 123, 2121

Stoughton C. et al., 2002, AJ, 123, 485 (EDR)

Strauss M.A. et al., 2002, AJ, 124, 1810

Strateva I. et al., 2002, AJ, 122, 1861

Syer D., Mao S., Mo H.J., 1999, MNRAS, 305, 357

Toomre A., Toomre J., 1972, ApJ, 178, 623

Thomas D., Maraston C., Bender R., 2002, Ap&SS, 281, 371

Trujillo I., Graham A.W., Caon N., 2001, MNRAS, 326, 869

van den Bosch F.C., 1998, ApJ, 507, 601

Warren M.S., Quinn P.J., Salmon J.K., Zurek W.H., 1992, ApJ, 399, 405

White S.D.M., Frenk C.S., 1991, ApJ, 379, 52

Wyse R.F.G., Gilmore G., Franx M., 1997, ARA&A, 35, 637

Yip C.W. et al., 2003, in preparation

York D. et al., 2000, AJ, 120, 1579